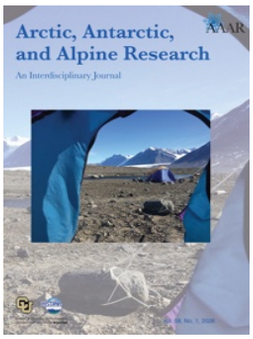

Taylor & Francis
Taylor & Francis Group

Arctic, Antarctic, and Alpine Research
An Interdisciplinary Journal

ISSN: 1523-0430 (Print) 1938-4246 (Online) Journal homepage: www.tandfonline.com/journals/uaar20

Chronology, cryostratigraphy, and palaeoenvironmental evidence from the CRREL Permafrost Tunnel, Alaska

Alistair J. Monteath, Scott L. Cocker, Thomas A. Douglas, Mikhail Kanevskiy , Michael F.J. Pisaric, Yuri Shur , Matthew J. Wooller & Duane Froese

To cite this article: Alistair J. Monteath, Scott L. Cocker, Thomas A. Douglas, Mikhail Kanevskiy , Michael F.J. Pisaric, Yuri Shur , Matthew J. Wooller & Duane Froese (2026) Chronology, cryostratigraphy, and palaeoenvironmental evidence from the CRREL Permafrost Tunnel, Alaska, Arctic, Antarctic, and Alpine Research, 58:1, 2677383, DOI: 10.1080/15230430.2026.2677383

To link to this article: https://doi.org/10.1080/15230430.2026.2677383

ARCTIC, ANTARCTIC, AND ALPINE RESEARCH
2026, VOL. 58, NO. 1, 2677383
https://doi.org/10.1080/15230430.2026.2677383

Chronology, cryostratigraphy, and palaeoenvironmental evidence from the CRREL Permafrost Tunnel, Alaska

Alistair J. Monteath[a], Scott L. Cocker[b], Thomas A. Douglas[c], Mikhail Kanevskiy[d], Michael F.J. Pisaric[e], Yuri Shur[d], Matthew J. Wooller[f], and Duane Froese[g]

[a]British Antarctic Survey, Natural Environment Research Council, Cambridge, UK; [b]Department of Geological Sciences, Stockholm University, Stockholm, Sweden; [c]U.S. Army Cold Regions Research and Engineering Laboratory (CRREL), Fort Wainwright, Alaska, USA; [d]Institute of Northern Engineering, University of Alaska Fairbanks, Fairbanks, Alaska, USA; [e]Department of Geography and Tourism Studies, Brock University, St. Catharines, Ontario, Canada; [f]Water and Environmental Research Center and College of Fisheries and Ocean Sciences, University of Alaska Fairbanks, Fairbanks, Alaska, USA; [g]Department of Earth and Atmospheric Sciences, University of Alberta, Edmonton, Alberta, Canada

ABSTRACT

The Cold Regions Research and Engineering Laboratory Permafrost Tunnel (CRREL Tunnel) in Alaska is one of the best studied Yedoma sequences in North America and is an exceptional site for understanding ice-rich, syngenetic permafrost. Here, we present cryostratigraphy, chronology, and stable isotopic analyses from eight exposures within the tunnel. These data are combined with previous studies to develop a composite sedimentary history and palaeoenvironmental record. At the sequence base, Fox Gravels were deposited ca. 45,000 calibrated years before C.E. 1950 (cal yr BP) and are overlain by silt that began accumulating ca. 43,000 cal yr BP. A slowing of silt accumulation (and possible hiatus) occurred ca. 36,000 cal yr BP and is associated with higher pore ice $\delta^{18}O$ values and thermokarst cave ice. Previous radiocarbon dates on ice wedge CO_2 from this unit are shown to be inaccurate, highlighting the difficulty in dating these features. Silt accumulation reactivated between 35,000–31,000 cal yr BP, with higher $\delta^{15}N$ values, suggesting more arid conditions. Published palaeoenvironmental data, placed in our new chronology, show shrub tundra was present between 43,000–41,000 cal yr. By 36,000 cal yr BP herbs and sedges replaced shrub tundra as the Bering Land Bridge became established.

ARTICLE HISTORY
Received 24 November 2025
Revised 7 May 2026
Accepted 14 May 2026

KEYWORDS
Chronology; permafrost; cryostratigraphy; Palaeoenvironments; Beringia

Introduction

Perennially frozen deposits (i.e., permafrost) have persisted in Beringia (unglaciated Alaska, Yukon, Siberia and exposed Chukchi/Bering continental shelf) for >700,000 years and provide important archives for a range of palaeoenvironmental and ground ice information (Froese et al. 2008; Murton et al. 2022). These deposits are best known for the preservation of megafaunal (animals weighing ≥44 kg) remains, including frozen mummies (Guthrie 1990); however, they also contain rich ecological (Murchie et al. 2021; Zazula et al. 2003), volcanic (Froese et al. 2002), and stable isotopic records (Monteath et al. 2023; Porter et al. 2016). In eastern Beringia (unglaciated Alaska and western Yukon), permafrost exposures exceed the time-period spanned by most lake records, which were often dry prior to ca. 15,000 calibrated years before C.E. 1950 (Hopkins 1982), and can be robustly dated through tephrochronology, optically stimulated luminescence, and careful selection of terrestrial plant macrofossils for radiocarbon dating (Preece et al. 2000; Westgate et al. 2001). These records therefore provide exceptional archives for understanding late Quaternary ecosystems and environmental processes (Froese et al. 2009).

Recently, several studies have examined palaeoenvironmental evidence and ground ice properties from permafrost deposits exposed by tunnels excavated into Quaternary sediments (Douglas et al. 2025; Iizuka et al. 2019; Meyer et al. 2008, 2010a, 2010b; Schirrmeister et al. 2016a). These allow extensive cryostratigraphic sequences spanning tens of thousands of years (or more) to be investigated at a single site. The most well-known example is the Cold Regions Research and Engineering Laboratory Permafrost Tunnel (CRREL

CONTACT Alistair Monteath alitea@bas.ac.uk British Antarctic Survey, Natural Environment Research Council, Cambridge, UK
Supplemental data for this article can be accessed online at https://doi.org/10.1080/15230430.2026.2677383

Tunnel) in Fox (Figure 1), 16 km north of Fairbanks, Alaska (64.951′N, 147.621′W). This large (500 m of excavated tunnels) tunnel complex provides a rare natural laboratory for understanding ice-rich, syngenetic permafrost and is one of the best studied Yedoma (fine grained, ice rich deposits associated with aggrading permafrost) sequences in North America (Kanevskiy et al. 2022; and references therein). However, the palaeoenvironmental record from the CRREL Tunnel remains comparatively underdeveloped. Although stable isotopic and ecological data provide detailed environmental snapshots, there has been no attempt to develop a well-dated continuous or semi-continuous palaeo-record from the site (Douglas et al. 2025; Griffing 2011; Hamilton, Craig, and Sellmann 1988; Lachniet, Lawson, and Sloat 2012; Lachniet et al. 2016; Sellmann 1967, 1972; Sloat 2014; Wooller et al. 2007, 2011).

Radiocarbon dating from a series of studies shows the CRREL Tunnel dissects a frozen sedimentary sequence that spans approximately 45,000–10,000 cal yr BP (Table S3). This time-period includes the Middle Wisconsin interstadial (approximately 57,000–30,000 cal yr BP) which is broadly coeval with the Karginsky interstadial in western Beringia (Anderson and Lozhkin 2001), and Marine Isotope Stage 3 (MIS3) globally. MIS3 is part of an unusual, Northern Hemisphere summer-insolation optimum that was one of the lowest amplitudes of recent Quaternary warm-stages (Berger and Loutre 1991). In eastern Beringia, well dated palaeoenvironmental records spanning this period are rare, with few exceptions (Gaglioti et al. 2018; Matthews Jr. 1974), and little is known about the climate or vegetation beyond approximately dated pollen records (Anderson and Lozhkin 2001; Monteath et al. 2025). Younger deposits in the CRREL Tunnel span the Pleistocene-Holocene transition (approximately 16,000–10,000 cal yr BP). This period of rapid environmental change coincided with the arrival of early paleolithic communities (ca. 14,000 cal yr BP; Potter et al. 2017) and the collapse of the steppe-tundra (mammoth steppe) ecosystem as grazing megafauna were extirpated and herbaceous, graminoid vegetation was replaced by first shrub tundra, then boreal forest (Guthrie 2001; Mann et al. 2002, 2013; Monteath et al. 2021, 2023; Murchie et al. 2021).

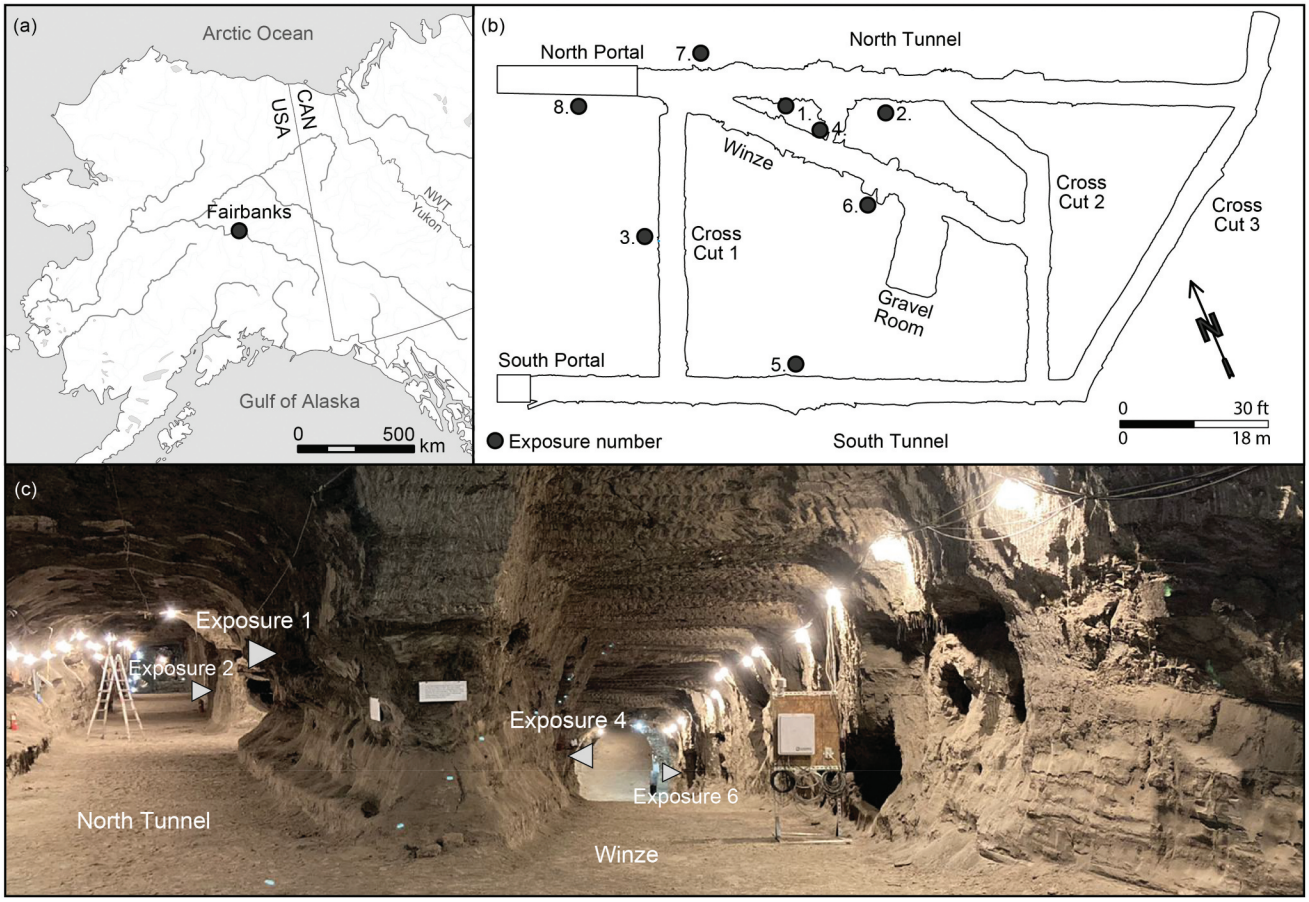

Figure 1. (a) The position of the CRREL Tunnel. (b) Plan view of the CRREL Tunnel and exposures described in this study. (c) Photograph taken from just beyond the North Portal, looking into the North Tunnel (on the left) and the Winze (descending ramp; on the right) and showing the positions of exposures one, two, four and six.

New work, combining modern precipitation and ground ice isotopic measurements from the CRREL Tunnel has shown that $\delta^{18}O$ and $\delta^{2}H$ values from pore-ice, wedge-ice and thermokarst cave-ice preserved in the tunnel sediments fall along the Local Meteoric Water Line (LMWL), and are climatically sensitive (Fig. S3; Douglas et al. 2025). Therefore, the CRREL Tunnel represents a rare archive of high-latitude MIS3 environments. In this study, we present stratigraphic descriptions, chronology and stable isotopic measurements ($\delta^{2}H$, $\delta^{18}O$, $\delta^{13}C$ and $\delta^{15}N$ values) from eight exposures in different sections of the CRREL Tunnel and place these within an overall site stratigraphy to develop a semi-continuous late Pleistocene environmental record.

The history and setting of the CRREL Tunnel

The CRREL Tunnel consists of three northwest-southeast tunnels each of which extends for >100 m: the North Tunnel, South Tunnel and Winze (descending ramp). These are around 4 m in height and are connected by three cross cutting tunnels. The North Tunnel and South Tunnel are excavated horizontally into the silt, whereas the Winze (descending ramp) slopes downward into the Gravel Room which is stratigraphically (and physically) below other tunnel sections at the CRREL Tunnel. It then rises to meet Cross Cut 2 (Figures 1, 2).

The first excavations of the CRREL Tunnel were undertaken by the U.S Army between 1963–1969. Initially, the North Tunnel and Winze were drilled into a 10 m high, northwest facing escarpment formed by placer gold mining activities in the Goldstream valley during the early- and mid-1900s. Subsequently, the tunnel complex was expanded in 2011–2013 and again in 2018–2021. The Quaternary stratigraphy of the North Tunnel, Winze and Gravel Room were first described and radiocarbon dated by Sellmann (1967,

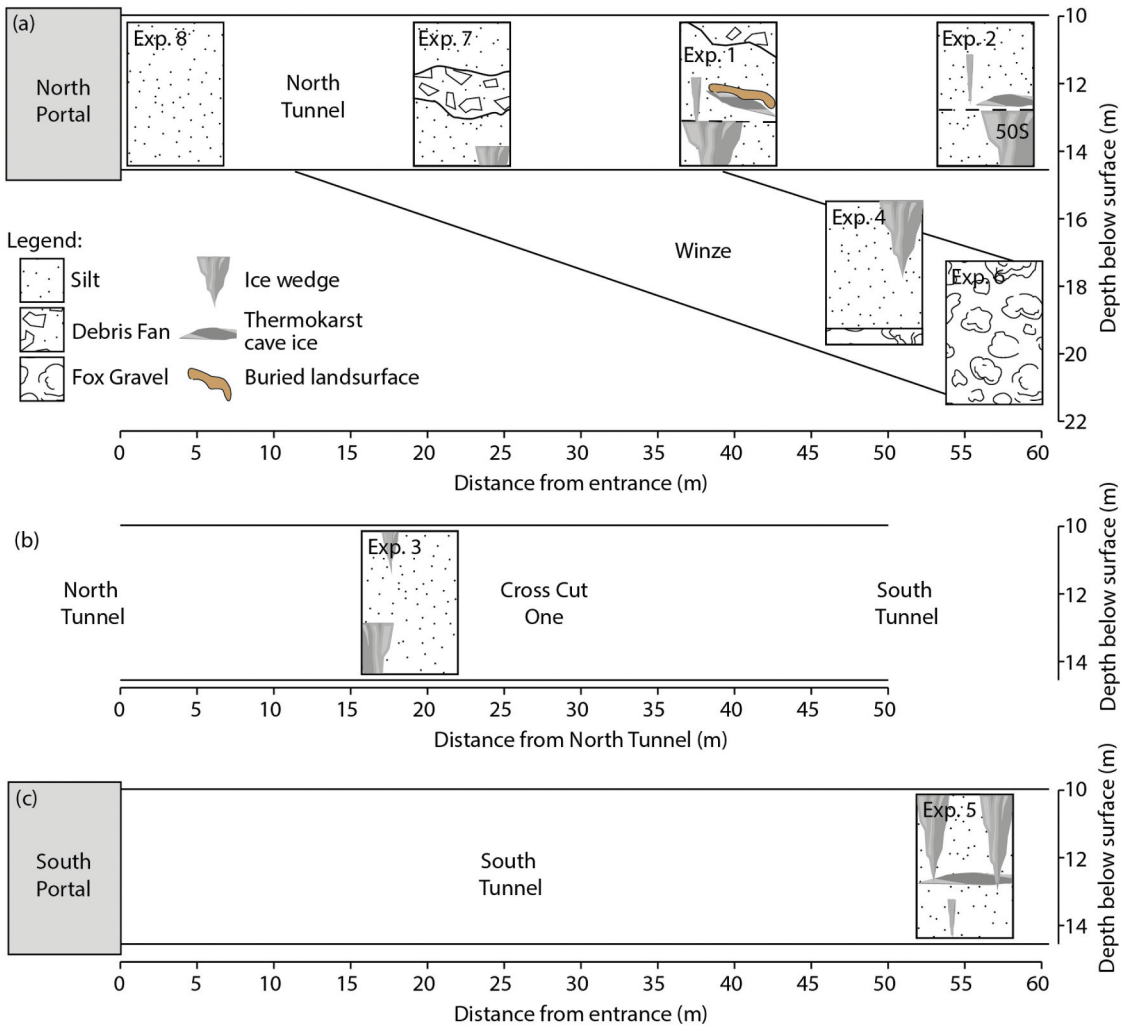

Figure 2. Schematic diagrams of the North Tunnel, South Tunnel and Cross Cut Tunnel, shown with stratigraphic logs of exposures examined in this study.

1972) and Hamilton, Craig, and Sellmann (1988). New excavations, including the 110 m South Tunnel and Cross Cut tunnels are described and dated by Kanevskiy et al. (2022).

The CRREL Permafrost Tunnel complex is situated near the southern margin of the Yukon-Tanana Upland and lies within the discontinuous permafrost zone (Jorgenson et al. 2008). The regional climate is continental (Köppen Climate Classification Dfc) with a mean annual air temperature of −2°C and monthly mean temperatures ranging between 20°C in summer to −20°C in winter. Measured seasonal extremes range from 38°C to −51°C (Jorgenson et al. 2001, 2020). The typical annual precipitation is 28 cm of water equivalent of which ~45 percent falls as snow (Liston and Hiemstra 2011). Annual temperature in the Fairbanks region has warmed 1.5°C since the 1970s (Fairbanks Airport station; Alaska Climate Research Center 2022) and during this time the length of the summer growing season has increased by 38 days (Wendler and Shulski 2009). This has led to widespread permafrost thaw throughout the region, including above the CRREL Tunnel (Douglas et al. 2021).

Quaternary cryostratigraphy of the CRREL Tunnel

The CRREL Tunnel dissects late Quaternary sediments that lie above frozen bedrock composed of pre-Cambrian, muscovite-quartz Fairbanks Schist (Newberry et al. 1996). The schist is only exposed in the lowest reaches of the Gravel Room and is ice-poor (average gravimetric moisture content 11.7 percent; Hamilton, Craig, and Sellmann 1988). Above this, the Fox Gravel forms a 3–4 m deposit composed of ice poor (average gravimetric moisture content 19.9 percent; Kanevskiy et al. 2022), imbricated sandy gravel, interstratified with layers and lenses of gravelly sand (Péwé 1975). Sand lenses often contain *Salix* wood, including rooted stumps, some of which may be in growth position (Hamilton, Craig, and Sellmann 1988). Three conventional radiocarbon dates and one liquid scintillation counting radiocarbon date from woody macrofossils in this unit suggest the Fox Gravels were deposited during MIS3, ca. 45,000 cal yr BP (Table S3), although these lie close to the practical limit of radiocarbon dating and must be treated with caution (Hamilton, Craig, and Sellmann 1988; Long and Péwé 1996).

Above the Fox Gravel, silt are present throughout the CRREL Permafrost Tunnel complex and are 14–17 m thick. The silt was subdivided into two depositional units by Sellmann (1967, 1972) and Hamilton, Craig, and Sellmann (1988) who describe an erosional/thaw event between them; the (1) lower silt and the (2) upper silt. The lower silt unit is ~4.5 m thick and includes large ice-wedges, up to 2 m wide, that have been truncated by a thaw/erosional event at a consistent height throughout the North Tunnel. Organic content in the lower silt is marginally higher (average 6.3 percent) than the upper silt (average 4.3 percent) and includes more frequent, and larger, woody remains (Hamilton, Craig, and Sellmann 1988). Shur et al. (2004) and Kanevskiy et al. (2022), however, argue that the silt deposits can be combined into one continuous unit based on the vertical extent of ice wedges in the South Tunnel (floor to ceiling) and boreholes, as well as variable ice wedge truncation heights exposed by new excavations in the South Tunnel and Cross Cut tunnels. Instead, Shur et al. (2004), Bray, French, and Shur (2006) and Kanevskiy et al. (2022) attributed thaw unconformities and the truncation of ice wedges to local thermokarst and thermo-erosional events. Repeated radiocarbon dating of different materials (Table S3) shows that the silt dates to MIS3 (Sellmann 1967, 1972; Hamilton, Craig, and Sellmann 1988; Kanevskiy et al. 2022). The age of ice wedges dissecting the silt is less clear and have been ascribed to both MIS3 (Hamilton, Craig, and Sellmann 1988; Sellmann 1967) and MIS2 (Lachniet, Lawson, and Sloat 2012).

In the North Tunnel, MIS3 silt is overlain by poorly sorted gravel with diamicton interbeds. This deposit is exposed in the wall near the North Portal and in the ceiling until ~40 m along the tunnel. The deposit was carefully studied by Hamilton, Craig, and Sellmann (1988) who interpreted it as a debris fan deposit and sub-divided the material into two sub-units; the upper fan and the lower fan. Kanevskiy et al. (2022) suggested that the entire deposit formed during deep erosion of the Goldstream Creek valley slopes which was quickly filled by streams and mudflows during the Pleistocene-Holocene transition. The fan deposits include cobbles and subangular pebbles of quartz and schist that are supported in a poorly sorted, sandy-silt/silty-sand matrix. Platy clasts are typically dipping and lie parallel to the bed. In places, roll structures are evident, indicating mass movement. The lower fan sub-unit includes silt with abundant shrub wood and thin lenses of organic matter that fill channel-like depressions in the underlying MIS3 silt. The upper fan sub-unit is clast rich and includes megafaunal (animals weighing >44 kg) fossils and wood logs (up to ~15 cm thick) amongst the rubble. Radiocarbon dates from woody shrub remains (*Salix*), snail shells and plant remains (undiff.) in the debris fan date to between 14,880–13,500 cal yr BP (Hamilton, Craig, and Sellmann 1988; Nield et al. 2024; Sellmann

1967), while bone remains date to 17,400–16,300 cal yr BP (Sellmann 1967). This offset is suggested to result from early methodological limitations in radiocarbon dating bones (Hamilton, Craig, and Sellmann 1988).

Finally, exposures within the vertical ventilation shaft (now inaccessible) and boreholes show that the CRREL Tunnel is overlain by Yedoma silt reworked by thermokarst and thermal erosion during the Holocene. Seven radiocarbon dates indicate that deposition occurred during the Early-Mid Holocene (Table S3). The unit includes 3–6 m of relatively ice-poor silt with peat horizons and organic matter inclusions. Thin ice wedges (0.1 to 1.0 m thick) are present as well as layers with micro-cryostructures (presumably syngenetically frozen soils or buried intermediate layers; Hamilton, Craig, and Sellmann 1988; Kanevskiy et al. 2022; Sellmann 1967).

Methods

In April 2022, we examined and sampled eight exposures from different sections of the CRREL Tunnel (Figures 1, 2). Lateral permafrost cores were collected from each exposure using either a three- or one inch diameter corer, driven by an electric-powered drill. Cores, macrofossil samples (woody shrub remains), and fossils (woolly mammoth [*Mammuthus primigenius*] tusk, steppe-bison [*Bison priscus*] horn sheath, and bone) were shipped frozen to the Permafrost Archive Science Laboratory (PACS), University of Alberta, Canada, and stored at −25°C.

Radiocarbon dating

We prepared 31 macrofossil samples from the CRREL Permafrost Tunnel for Accelerator Mass Spectrometry (AMS) radiocarbon dating (Table 1, S2) alongside subsamples of well-characterized standards of comparable mass. These standards included AVR-PAL-07, an internal standard of last interglacial age to establish background radiocarbon abundance (De Martinez et al. 2019), and two well-dated Holocene international standards to verify age quality; FIRI-F and IAEA-C5. Pretreatment of all samples followed standard acid-base-acid procedures (e.g., Reyes, Froese, and Jensen 2010). Samples were placed on a heating block at 70°C and submerged in 1 M HCl for 30 minutes, followed by successive 30-minute treatments in 1 M NaOH until the liquid remained clear. Samples were then submerged in a final 1 M HCl treatment for 30 minutes followed by successive 15-minute rinses in ultrapure water until pH > 6. Ultra-fine tip pipettes were used on low mass samples to mitigate losses. Samples were then frozen, freeze-

Table 1. Radiocarbon (^{14}C) dates from the CRREL Permafrost Tunnel measured in this study. Dates were calibrated using OxCal v.4.4 and the IntCal20 radiocarbon calibration curve (Bronk Ramsey 2009a; Reimer et al. 2020).

Location	Exposure	Sample	Lab n.	Age (^{14}C yr BP)	Age (cal yr BP)	Median (cal yr BP)	Material
North tunnel	1	SC22-1-10	UCIAMS-265201	33,520 ± 550	39,751–36,883	38,343	Plant macrofossil undif.
North tunnel	1	SC22-1-14C A	UCIAMS-265035	31,430 ± 200	36,200–35,369	35,800	*In situ* graminoid
North tunnel	1	SC22-1-14C B	UCIAMS-265034	31,960 ± 210	36,860–35,875	36,309	*In situ* graminoid
North tunnel	1	SC22-1-14C C	UCIAMS-265040	31,080 ± 190	36,033–34,910	35,471	*In situ* graminoid
North tunnel	1	SC22-1-15	UCIAMS-265200	31,690 ± 230	36,473–35,456	36,033	Plant macrofossil undif.
North tunnel	1	SC22-1-5	UCIAMS-265199	32,100 ± 1500	40,871–34,227	37,078	Plant macrofossil undif.
North tunnel	2	SC22-2-43	UCIAMS-265039	40,090 ± 540	44,290–42,680	43,384	Plant macrofossil undif.
North tunnel	2	SC22-2-45-bulk	UCIAMS-265048	38,580 ± 450	42,887–42,149	42,491	Plant macrofossil undif.
North tunnel	2	SC22-2-46	UCIAMS-265038	38,790 ± 460	42,995–42,208	42,572	Plant macrofossil undif.
North tunnel	2	SC22-2-51	UCIAMS-265194	31,770 ± 350	36,875–35,395	36,117	Plant macrofossil undif.
North tunnel	2	SC22-2-53	UCIAMS-265195	27,120 ± 180	31,574–31,012	31,193	Plant macrofossil undif.
North tunnel	2	SC22-2-55	UCIAMS-265043	28,700 ± 140	33,622–32,255	33,071	Plant macrofossil undif.
Cross Cut One	3	SC22-3-63	UCIAMS-265204	32,860 ± 260	38,449–36,514	37,304	Graminoid rootlets
Cross Cut One	3	SC22-3-70	UCIAMS-265045	32,050 ± 220	36,935–36,008	36,397	*In situ* shrub wood
Winze	4	SC22-4-79	UCIAMS-265203	39,380 ± 580	43,974–42,343	42,879	Plant macrofossil undif.
Winze	4	SC22-4-83	UCIAMS-265196	39,750 ± 600	44,193–42,480	43,144	Graminoid rootlets
South tunnel	5	SC22-5-71	UCIAMS-265202	32,840 ± 260	38,399–36,489	37,275	Plant macrofossil undif.
South tunnel	5	SC22-5-73	UCIAMS-265197	30,880 ± 470	36,192–34,462	35,278	Graminoid rootlets
South tunnel	5	SC22-5-78 A	UCIAMS-265046	30,640 ± 180	35,380–34,600	34,995	*Salix* leaves
South tunnel	5	SC22-5-78 B	UCIAMS-265037	30,510 ± 170	35,293–34,535	34,903	*Salix* leaves
Winze	6	SC22-6-84 A	UCIAMS-265047	43,280 ± 800	47,546–44,566	45,790	Wood
Winze	6	SC22-6-84 B	UCIAMS-265036	42,560 ± 740	46,695–44,205	45,222	Wood
North tunnel	7	SC22-7-87	UCIAMS-265198	33,200 ± 1700	41,907–34,915	38,238	Plant macrofossil undif.
North tunnel	7	SC22-7-90 A	UCIAMS-265041	11,960 ± 35	14,023–13,760	13,862	*Salix* wood
North tunnel	7	SC22-7-90 B	UCIAMS-265044	11,850 ± 25	13,784–13,606	13,690	*Salix* wood
North tunnel	7	SC22-7-91 A	UCIAMS-265042	11,900 ± 25	13,984–13,606	13,767	*Salix* wood
North tunnel	7	SC22-7-91 B	UCIAMS-265033	11,790 ± 25	13,755–13,521	13,657	*Salix* wood
North tunnel	7	SC22-7-94	UCIAMS-265029	13,605 ± 40	16,586–16,284	16,427	Bison scapula
North tunnel	7	SC22-7-95	UCIAMS-265223	23,530 ± 90	27,854–27,458	27,719	Bison horn sheath
North tunnel	7	SC22-7-96	UCIAMS-265030	13,350 ± 45	16,235–15,880	16,065	Mammoth tusk
North tunnel	8	SC22-8-97	UCIAMS-265031	14,295 ± 45	17,692–17,105	17,377	Bone undif.

dried overnight, and stored in airtight sterilized vials. CO_2 production, graphitization, and measurement of radiocarbon abundance of all samples were completed at the Keck-Carbon Cycle AMS facility (UCIAMS). Collagen from three megafauna fossils were prepared for radiocarbon dating using ultrafiltration (Brown et al. 1988) at UCIAMS. Keratin from a fragment of steppe-bison horn sheath was treated using acid-base-acid protocols at UCIAMS.

Bayesian age modeling

We combined chronological data within Bayesian age models using OxCal v.4.4 and the Northern Hemisphere IntCal20 radiocarbon calibration curve (Bronk Ramsey 2009a; Reimer et al. 2020). For each exposure, we developed a P_Sequence depositional model (Fig. S4) and applied a variable k parameter (depositional events per unit length: cm^{-1}) and a General_Outlier model (Bronk Ramsey 2008, 2009b; Bronk Ramsey and Lee 2013). Where the stratigraphic relationship between exposures was known (e.g., exposure two lies stratigraphically above exposure four, which lies above exposure six) P_Sequence depositional models were nested within a Sequence model so that chronological data from multiple exposures could be combined. Individual radiocarbon dates were assigned a five percent prior probability (i.e., one in twenty) of being an outlier. Throughout the manuscript modeled age ranges are reported as median ages or at two sigma (95.4 percent) level confidence. OxCal code for each age-depth model is reported in Supplementary Information.

To determine the timing of stable water isotopic (δ^2H and $\delta^{18}O$ values) changes in relict pore-water a pore-ice-specific age-depth model that includes some understanding of the palaeo-active layer thickness is required (Porter and Opel 2020). Syngenetic pore-ice represents meteoric waters that infiltrated the active layer and froze *in situ* before being preserved by the aggrading permafrost table. This process is paced by the rate of sediment accumulation at the surface and so the depositional age of the pore-ice is always younger than the host sediments. Monteath et al. (2023) and Cocker et al. (2026) both used a combination of modern measurements and palaeoenvironmental evidence from arctic ground squirrel (*Urocitellus parryii*) middens and paleosols to infer palaeo-active layers. The end members from these data were then used to test the sensitivity of chosen active layer depths on the pore-ice chronology. Active layer depth data from interior Alaska during the MIS3 and the latest Pleistocene are unavailable but are likely to have been at least as deep as today (Guthrie 2001). Present active layer depths around Fairbanks, Alaska, are typically 20–80 cm (Douglas et al. 2008) and thaw measurements taken between C.E. 1946–1972 were consistently ~85 cm (Linell 1973). We therefore applied a palaeo-active layer of 85 cm to our samples. Given the rapid silt accumulation rate (0.04–0.27 mm yr^{-1}; Table S1) the choice of palaeo-active layer depths is unlikely to affect the modeled age of pore-ice by more than decades-to-centuries; well within the two-sigma uncertainties of the Bayesian age-depth models.

Pore-ice $\delta^2H/\delta^{18}O$ measurements

We measured ground ice δ^2H and $\delta^{18}O$ values using a Picarro (model L2130-i) water isotope analyzer (Fig. S5). Raw δ^2H and $\delta^{18}O$ values were normalized to the VSMOW-SLAP scale using reference water samples USGS-45 (δD = –10.3‰, $\delta^{18}O$ = –2.2‰) and USGS-46 (δD = –235.8‰, $\delta^{18}O$ = –29.8‰). Fifteen replicate analyses were undertaken on samples from the CRREL Tunnel to demonstrate consistency between runs. Analytical precision in this study was 0.5‰ for δ^2H values and 0.2‰ for $\delta^{18}O$ values based on routine measurement of an internal secondary water standard.

Particle size analysis

We measured particle size using laser diffraction with a Malvern Mastersizer 3000. Before analysis, oven dried samples were burnt at 550°C for two hours and then mixed with a weak dispersant solution of five percent Sodium hexametaphosphate (Calgon) to form a homogenous paste (Konert and Vandenberghe 1997). Samples were weighed before and after burning to provide a measurement of organic content (Heiri, Lotter, and Lemcke 2001). For each analysis settings were adjusted so that the standard deviation of these five measurements was below five percent for the D10, D50, and D90 values. These adjustments included: adding more sample material to increase obscuration and/or the application of ultrasound.

Percentage N, C and $\delta^{13}C$, $\delta^{15}N$ measurements

We determined %C, %N, $\delta^{13}C$, and $\delta^{15}N$ values using a Thermo Scientific Flash Elemental Analyzer attached via a Thermo Scientific Conflo IV to a Thermo Scientific Delta V plus Isotope Ratio Mass Spectrometer at the Alaska Stable Isotope Facility, University of Alaska, Fairbanks. Samples of weighed, freeze-dried sediment were placed in tin capsules and sealed prior to C and N measurements. Analysis followed standard protocols

(Wooller et al. 2007) and results are presented as standard delta (δ) notation as well as relative to the Vienna Pee Dee Belemnite (VPDB) and air, respectively. The analytical precision (defined here as 1 standard deviation calculated from seven analyses of peptone as an internal laboratory standard) for %C, %N, $\delta^{13}C$, and $\delta^{15}N$ were 0.4 percent, 0.4 percent, 0.1 percent, and 0.1 percent, respectively. In eastern Beringia, changes in Yedoma $\delta^{15}N$ values are thought to be primarily controlled by soil moisture, although this relationship is difficult to quantify (Handley et al. 1999; Rabanus-Wallace et al. 2017).

Macrofossil analysis

To identify woody macrofossil remains, we undertook thin section analysis on samples collected from Debris Fan deposits that are evident in the tunnel wall near the North Portal (SC22-7-90, Sample E and SC22-7-90, Sample D) l. For each macrofossil we produced 10–15 mm thin sections in the transversal, tangential, and radial directions using the WSL Lab-Microtome (Fig. S2; Gärtner, Lucchinetti, and Schweingruber 2015). Wood characteristics used for identifying samples followed the keys and examples published in Schweingruber (2016).

Results

All eight exposures examined in this study can be placed in common cryostratigraphic units previously described by Hamilton, Craig, and Sellmann (1988) and Kanevskiy et al. (2022). The principal ground ice features (Fig. S1) encountered in this study are described following the nomenclature of Murton and French (1994) with modifications from our own experience and previous studies of the CRREL Tunnel (Supplementary Text S1).

Exposure one

Exposure one is located in the North Tunnel, 37–40 m from the portal entrance (Figures 1, 3), and includes a well preserved, vegetated land surface described by Wooller et al. (2007), Wooller et al. (2011). The 4 m exposure can be divided into two depositional sub-units, separated by an erosional contact, which were described by Hamilton, Craig, and Sellmann (1988) as the upper and lower silt. Sub-unit one is composed of silt with microlenticular cryostructure, that becomes finer grained toward the top of the unit (66–75 percent silt). Organic content varies between 4–8 percent, the average sediment $\delta^{15}N$ value is ~3.3 and $\delta^{18}O$ values for pore and segregated ice are consistently around –22.8‰. Pore ice Deuterium-excess (D-excess) values vary between 3.1

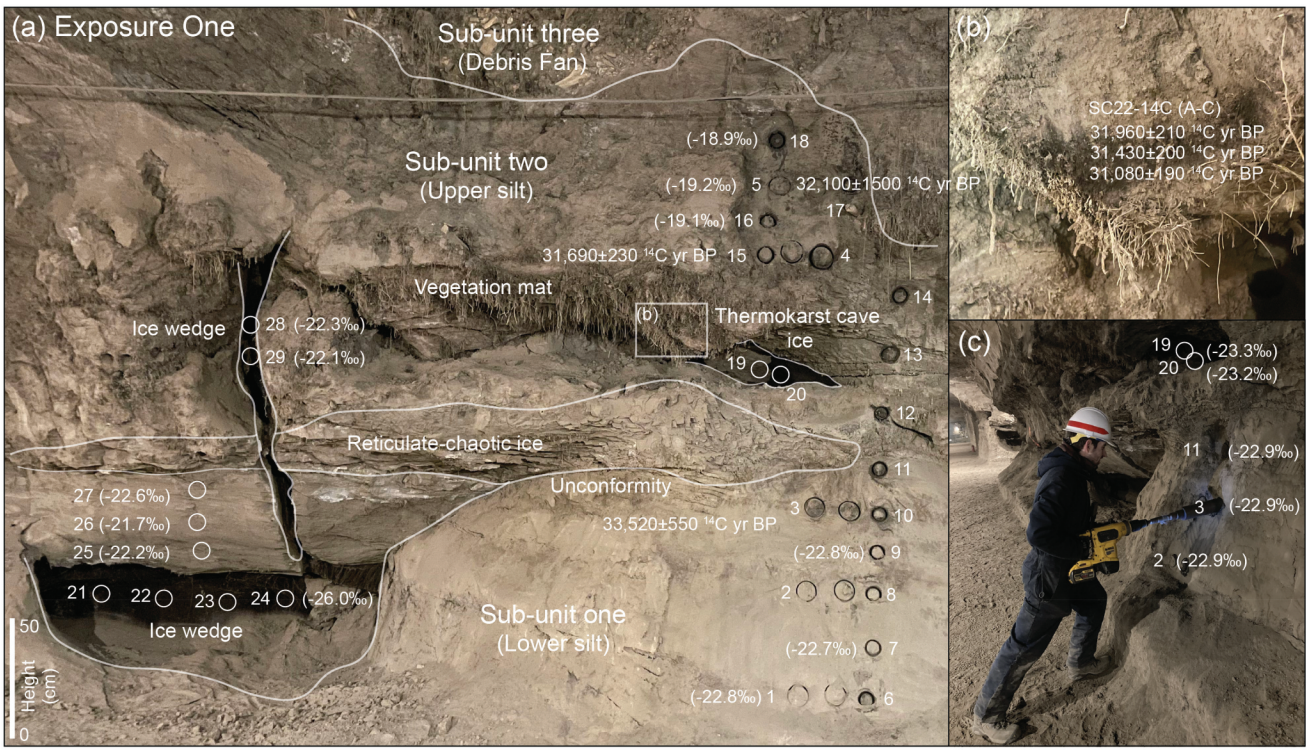

Figure 3. (a) Annotated image of Exposure One, North Tunnel, including selected isotopic ($\delta^{18}O$) and radiocarbon data. Sampling numbers refer to SC-22 labeling. (e.g., SC-22-1-1). (b) Paleosol associated with the vegetation mat. (c) Lateral coring Exposure one.

to –2.9 with higher values lower in the sub-unit. A radiocarbon date from the top of this sub-unit indicates that it was deposited prior to ca. 38,350 cal yr BP (SC22-1-10, 33,520 ± 550 ^{14}C yr BP). The sub-unit is separated from the overlying sediments by a sharp contact that marks an unconformity/re-working event and truncates a large ice wedge with low δ^{18}O values (mean –25.7‰). Sediments above the unconformity have chaotic-reticulate cryostructure overlain by thermokarst cave ice (mean –23.2‰ δ^{18}O value). A well-preserved vegetation mat is present as part of the unconformity and was described in detail by Wooller et al. (2007), Wooller et al. (2011). A graminoid leaf sample from this vegetation mat was radiocarbon dated to 36,490–35,330 cal yr BP (NOSAMS-49819, 31,600 ± 290 ^{14}C yr BP) by Wooller et al. (2011) and three new dates from *in situ* graminoid leaves sampled by this study confirm this age (SC22-1-14C-265035, 31,430 ± 200 ^{14}C yr BP, 31,960 ± 210 ^{14}C yr BP, 31,080 ± 190 ^{14}C yr BP). Above the unconformity, Sub-unit two is formed of silt with similar sediment δ^{15}N values (~3.0‰), but higher organic content (10–12 percent) and higher δ^{18}O values than the underlying sediments (–18.5 to –19.2‰). Pore ice D-excess values vary between 0.6 to 4.9 with higher values in the uppermost silt. A thin ice wedge with higher δ^{18}O values (–22.2‰) dissects the silt. The sequence is capped by poorly sorted gravels (Debris Fan) which diagonally truncate the exposure and include abundant, large woody macrofossils. Two radiocarbon dates from the silt are broadly in agreement with dates from the vegetated land surface (SC22-1-15, 31,690 ± 230 ^{14}C yr BP; SC22-1-5, 32,100 ± 1500 ^{14}C yr BP).

Exposure two

Exposure two is located in the North Tunnel (Figures 1, 4), 52–56 m from the entrance, and is immediately adjacent to a radiocarbon-dated ice wedge (50S) described by Lachniet, Lawson, and Sloat (2012). The 4.5 m high exposure includes two sub-units, separated by an erosional contact, which were described by Hamilton, Craig, and Sellmann (1988) as the upper and lower silt. Sub-unit one includes the lower 2.5 m of the exposure and is formed of silt (59–84 percent silt) with low sediment δ^{15}N values (~2.2‰) and variable organic content (6–23 percent). The δ^{18}O values from pore and segregated ice range between –22.7 to –20.7‰, become marginally lower toward the top of the sub-unit. Pore ice D-excess values vary between 0.1 to 3.2. Sub-unit one includes four paleosols—the most prominent of which can be traced for tens of meters along the tunnel walls (further into the North Tunnel and Cross Cut Two). The lowest of these paleosols is radiocarbon-dated to ca. 43,400 cal yr BP (SC22-2-43, 40,090 ± 540 ^{14}C yr BP), consistent with dating from exposure four in the Winze, which lies stratigraphically below exposure two (Figure 2). Sub-unit one is truncated by an unconformity represented by reticulate-chaotic cryostructure ice and an exposed section of thermokarst cave ice. δ^{18}O values from the cave ice are between –24.1 and –24.3‰. Above this, sub-unit two is composed of silt (65–78 percent silt) with lower organic content (4–13 percent), but higher sediment δ^{15}N values (~3.3) than underlying sub-unit one. Pore-ice δ^{18}O measurements become marginally higher toward the top of the sub-unit (–22.8 to –20.9‰). Pore ice D-excess values vary between 0.5 and 2.8, becoming lower toward the top of the sub-unit. A thin (approximately 15 cm wide) ice-wedge dissects sub-unit two (–21.5 to –21.2‰ δ^{18}O). The upper most samples did not include enough pore-ice and segregated ice for successful isotopic measurements. Embedded in the ceiling above exposure two, a vegetation mat is radiocarbon dated to ca. 33,100 cal yr BP (UCIAMS-265043, 28,700 ± 140 ^{14}C yr BP).

Exposure three

Exposure three is located in Cross Cut One and is composed of fine-grained (silt), massive sediments (67–78 percent silt), intermediate sediment δ^{15}N values (~3.0‰), high organic contents (9–21 percent) and large ice wedges either side of the sampled section (Figures 1, 5). A prominent paleosol is present at the base of the sequence and can be traced for tens of meters along the tunnel wall. Near the top of the exposure a large, woody plant macrofossil is present in what appears to be a growth position. δ^{18}O measurements are largely consistent throughout the section and vary between –21.6 and –19.9‰. Pore ice D-excess values vary between 0.7 to 3.0. Two radiocarbon dates from this study date exposure three to between ca. 37,304 cal yr BP and ca. 36,397 cal yr BP (SC22-3-63, 32,860 ± 260 ^{14}C yr BP; SC22-3-70, 32,050 ± 220 ^{14}C yr BP).

Exposure four

Exposure four is located in the Winze, 31 m from the North Portal, and is stratigraphically (and physically) bellow other exposures in CRREL Tunnel, with the exception of exposure six (Figures 1, 6). Fox Gravels are exposed at the base of the sequence and are overlain by silt with a moderate sand component (~30 percent). Organic content varies between 9–13 percent.

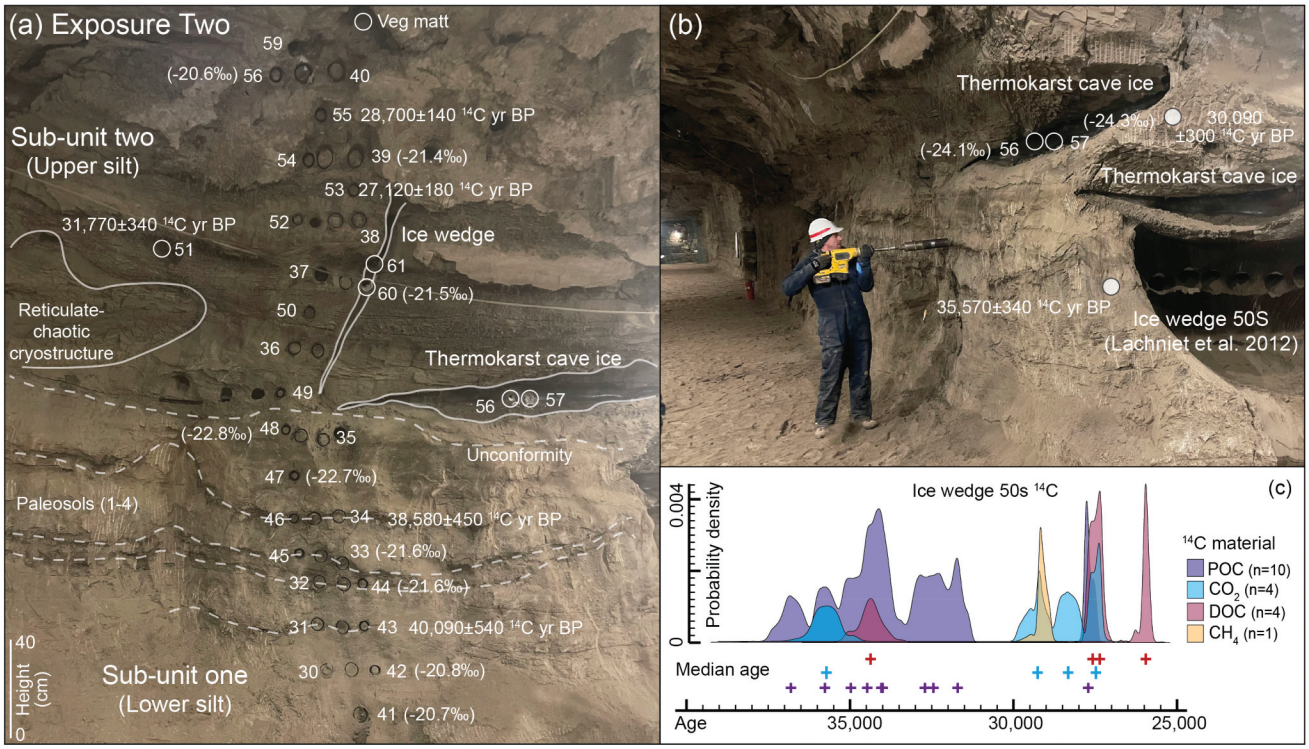

Figure 4. (a) Annotated image of Exposure Two, North Tunnel, including selected isotopic ($\delta^{18}O$) and radiocarbon data. Sampling numbers refer to SC-22 labeling. (e.g., SC-22-2-30). (b) Exposure Two shown in relation to ice wedge 50S that was extensively studied by Lachniet, Lawson, and Sloat (2012). Filled circles indicate data from Lachniet, Lawson, and Sloat (2012). (c) Sum probability of radiocarbon dating from ice wedge 50S. All 50S dates come from Lachniet, Lawson, and Sloat (2012) except for the CH_4 date which comes from Katayama et al. (2007).

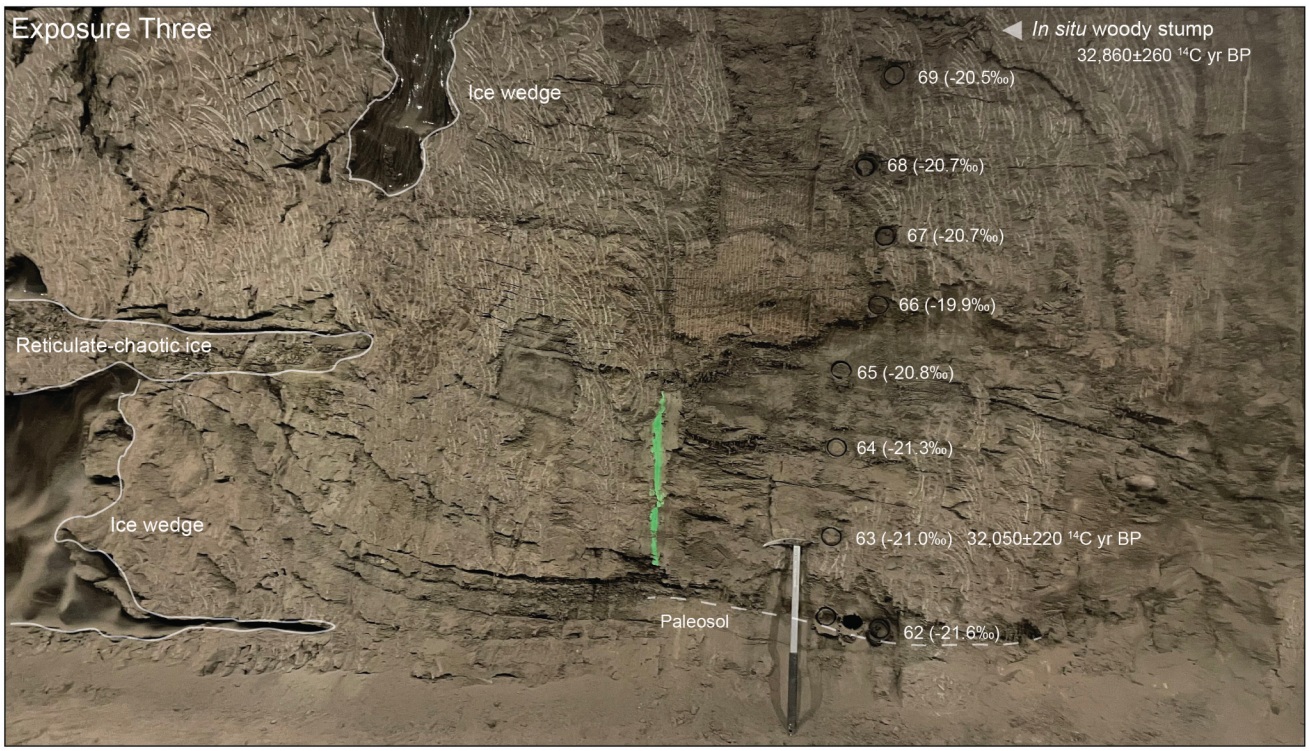

Figure 5. Annotated image of Exposure Three, Cross Cut One, including isotopic ($\delta^{18}O$) and radiocarbon data. Sampling numbers refer to SC-22 labeling. (e.g., SC-22-3-62).

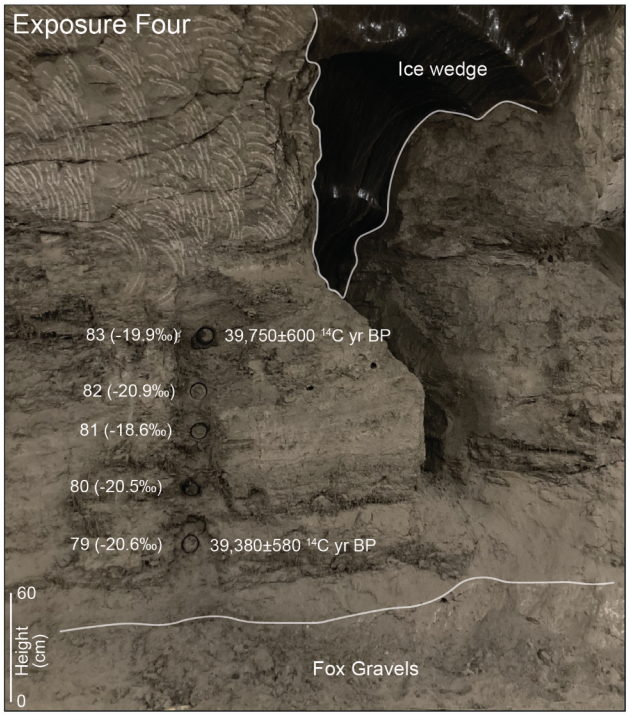

Figure 6. Annotated image of Exposure Four, Winze, including isotopic ($\delta^{18}O$) and radiocarbon data. Sampling numbers refer to SC-22 labeling (e.g., SC-22-4-79).

Floodplain organics and fluvial intrabeds are common near the base of the exposure, interbedded with the fine-grained (loessal) sediments. Pore ice $\delta^{18}O$ and organic content measurements are consistent throughout the exposure; varying between –18.6 and –20.9‰, and 9.6–12.8 percent, correspondingly. Pore ice D-excess values vary from –6.0 to 2.8. Sediment $\delta^{15}N$ values (~1.5‰) are lower than those measured in most other units. Two radiocarbon dates from this study date exposure four to ca. 43,000 cal yr BP (SC22-4-79, 39,380 ± 580 ^{14}C yr BP; SC22-4-83, 39,750 ± 600 ^{14}C yr BP). The sequence spans the local transition from fluvial to eolian deposition at the CRREL Tunnel.

Exposure five

Exposure five is located in the South Tunnel, 55 m from the South Portal (Figures 1, 7). The sediments are formed of silt (63–77 percent silt). with moderate organic content (9–13 percent) and low sediment $\delta^{15}N$ values (~1.8‰). Three pore-ice $\delta^{18}O$ values vary between –19.7 to –20.6‰, with D-excess values between –2.7 to 2.8. The sediments are dissected by a thin ice wedge (approximately 10 cm thick, –20.3‰ $\delta^{18}O$) as well as a 10–15 cm thick band of thermokarst cave ice (to –22.6‰ $\delta^{18}O$) that overlies chaotic-reticulate ice and is dissected by larger ice

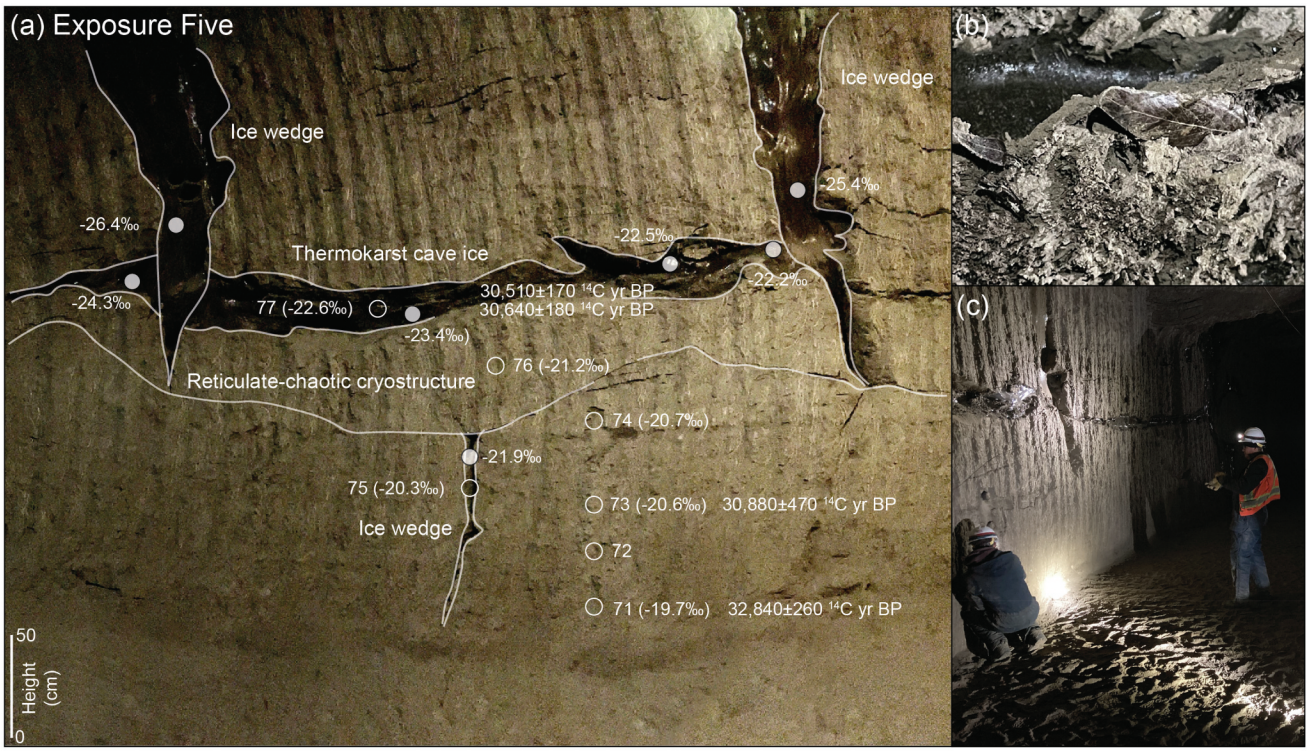

Figure 7. Annotated image of Exposure Five, South Tunnel, including isotopic ($\delta^{18}O$) and radiocarbon data. Sampling numbers refer to SC-22 labeling. (e.g., SC-22-3-62). Filled circles indicate data from Kanevskiy et al. (2022). (b) *Salix* leaves exposed by sublimating thermokarst cave ice. (c) Surveying and sampling Exposure Five.

wedges (–26.4 to –25.5‰ $\delta^{18}O$; Kanevskiy et al. 2022) that extend throughout the upper portion of the exposure. Within the thermokarst cave ice numerous *Salix* leaves are exceptionally well preserved, and are radiocarbon dated to ca. 34,950 cal yr BP (SC22-5-78, 30,640 ± 180 ^{14}C yr BP, 30,510 ± 170 ^{14}C yr BP). The base of Exposure five is radiocarbon-dated to ca. 37,300 cal yr BP (SC22-5-71, 32,840 ± 260 ^{14}C yr BP).

Exposure six

Exposure six is located in the Winze, 51 m from the North Tunnel portal, and is stratigraphically (and physically) bellow other exposures in CRREL Tunnel (Figures 1, 8). The exposure is formed entirely of Fox Gravel and includes large clasts interbedded with silty-sand deposits. Large *Salix* macrofossils are common in this deposit. No particle size, organic content, $\delta^{13}C$, $\delta^{15}N$, $\delta^{2}H$, or $\delta^{18}O$ values were made on this section. Two *Salix* wood samples from this deposit were radiocarbon-dated to ca. 45,000 cal yr BP (SC22-6-84, 43,280 ± 800 ^{14}C yr BP, 42,560 ± 740 ^{14}C yr BP).

Exposure seven

Exposure seven is located in the North Tunnel, 23 m from the tunnel entrance, and includes three sub-units

Figure 8. Annotated image of Exposure Six, Winze, including radiocarbon data.

(Figures 1, 9). Sub-unit one is formed of silt (75–83 percent silt) with moderate organic content (8–11 percent) and sediment $\delta^{15}N$ values (~2.6‰) and is dissected by one thin ice-wedge, partially obscured by sublimating silt at the base of the exposure (approximately 20 cm width). Four pore ice $\delta^{18}O$ measurements vary between –22.5 and –23.2‰. Pore ice D-excess values increase with height, from 0.6 to 5.1. One radiocarbon date from this sub-unit dates to ca. 38,200 cal yr BP (SC22-7-87, 33,200 ± 1700 ^{14}C yr BP). Sub-unit two is formed of coarser, sandy-silt (53 percent silt) with lower sediment $\delta^{15}N$ (~2.0) values, and includes large, angular cobles as well as abundant *Salix* wood which is dated to ca. 13,600 cal yr BP (SC22-7-90, 11960 ± 35 ^{14}C yr BP, 11,850 ± 25 ^{14}C yr BP;SC22-7-91, 11,900 ± 25 ^{14}C yr BP, 11,790 ± 25 ^{14}C yr BP). Megafauna (woolly mammoth and steppe-bison) fossils are also present in this sub-unit and are radiocarbon-dated to between 16,000–28,000 cal yr BP (SC22-7-94, 13,605 ± 40 ^{14}C yr BP; SC22-7-95, 23,530 ± 90 ^{14}C yr BP; SC22-7-96, 13,350 ± 45 ^{14}C yr BP). Finally, the exposure is capped by sub-unit three; formed of inorganic (5 percent), sandy-silt (66–55 percent silt) with higher $\delta^{18}O$ values (–18.9 to –19.6‰).

Exposure eight

Exposure eight is located in the North Tunnel, immediately adjacent to the tunnel entrance and has been heavily sampled by previous studies (Figures 1 and 10). The exposure is composed of massive silty-sediments (60 percent silt) that are coarser and less organic (4 percent organics) than other deposits in the CRREL tunnel complex. Sediment $\delta^{15}N$ values are variable (1.2–3.0‰). Ice content is low in this unit and the $\delta^{18}O$ of relict water was only successfully extracted from one sample which was measured as –18.5‰ $\delta^{18}O$ value (D-excess 0.6). The sediments are described as "slumped silt" by Hamilton, Craig, and Sellmann (1988). A bone fragment (likely steppe-bison scapula) was found, associated with sample SC22-8-97 and radiocarbon dated to ca. 17,400 cal yr BP (SC22-8-97, 14,295 ± 45 ^{14}C yr BP). This date provides a minimum age for the unit; however, it is unclear if the sub-fossil is *in situ* or was reworked from older sediments.

Discussion

Reexamining ice wedge radiocarbon dating

Ice wedges in the CRREL Tunnel have been linked with both MIS3 (Hamilton, Craig, and Sellmann 1988) and

Figure 9. (a) Annotated image of Exposure Seven, North Tunnel, including selected isotopic ($\delta^{18}O$) and radiocarbon data. Sampling numbers refer to SC-22 labeling (e.g., SC22-7-85). (b) Woolly mammoth sub-fossils. (c) Steppe-bison horn (both situated left of image A).

Figure 10. Annotated image of Exposure Eight, North Tunnel, including isotopic ($\delta^{18}O$) and radiocarbon data. Sampling numbers refer to SC-22 labeling (e.g., SC-22-8-97).

MIS2 (Lachniet, Lawson, and Sloat 2012). The strongest evidence for MIS2 ice wedge formation is presented by Lachniet, Lawson, and Sloat (2012) who radiocarbon dated different organic and gas fractions trapped within ice wedge 50S, immediately adjacent to exposure two in the North Tunnel (Figure 4). The study found that radiocarbon dates from particulate organic matter (POC) were consistently older than dates derived from dissolved organic carbon (DOC) or CO_2 (Figure 4), which were considered more reliable and used to infer that ice wedges throughout the CRREL Tunnel formed epigenetically during the Last Glacial Maximum (26,000–16,000 cal yr BP). In this study, we tested these findings by systematically dating deposits above and below wedge 50S at exposure two (Figure 4). Macrofossils from sediment below, and surrounding, ice wedge 50S are consistently radiocarbon dated to 43,000–38,000 cal yr BP and provide a maximum age for wedge formation, similar to the estimate of ca. 41,000 cal yr BP made by Lachniet, Lawson, and Sloat (2012). Above this, ice wedge 50S is truncated by thermokarst cave ice that extends into exposure two and is associated with reticulate-chaotic cryostructure (Figure 4). This erosional feature was suggested to date to 21,500–14,900 cal yr BP by Lachniet, Lawson, and Sloat (2012); however, at this point our interpretations differ. Our new radiocarbon dating and stratigraphic evidence for accumulation of

silt overlying wedge 50S indicates that the underlying ice wedge must be older than 36,000–33,000 cal yr BP. These two chronological models are not compatible and so we outline several lines of evidence that support our recommended chronological model and interpretation:

(1) Radiocarbon background measurements are essential for assessing the quality of dates that are near the temporal limit of the technique or based on low mass samples. Our new radiocarbon dates were measured alongside AVR-PAL-07, an internal standard of last interglacial age, to establish background radiocarbon abundance (De Martinez et al. 2019). This data is not available for dates reported in Lachniet, Lawson, and Sloat (2012) making it harder to assess accuracy.
(2) Radiocarbon dates on macrofossils retrieved from thermokarst cave ice by Lachniet, Lawson, and Sloat (2012), Kanevskiy et al. (2022) and this study (SC22-5-78) cluster around 36,000–35,000 cal yr BP. This includes two new dates on *Salix* leaves which both returned ages of ca. 36,000 cal yr BP. These fragile macrofossils are unlikely to have been reworked from older deposits (e.g., Kennedy et al. 2010) and add confidence that the true age of the thermokarst cave ice is between 35,000–36,000 cal yr BP. These lines of suggest that the ice formed during a brief period of thermokarst and thermal erosion that could represent a singular event (Figures 4, 12). This age agrees with the chronology of exposure two and the hiatus that affects wedge 50S, which is dated to 42,000–36,000 cal yr BP in this study.
(3) Five radiocarbon dates from exposure one overlie an ice wedge that is contemporaneous with wedge 50S and is one of a series of wedges that are truncated at the same height in the North Tunnel (Bray, French, and Shur 2006; Hamilton, Craig, and Sellmann 1988). These dates are consistent with dating by Wooller et al. (2011) on *in-situ* vegetation and indicate that the truncated wedges must be older than 36,000–35,000 ka.
(4) Wood immediately above wedge 50S was dated to ca. 35,000 by Lachniet, Lawson, and Sloat (2012) but considered to represent reworked material. This date is in good agreement with the chronology of exposure two and may accurately record the timing of thermokarst.

Our chronology is consistent between exposures and with stratigraphic and chronological data from elsewhere in the CRREL Tunnel. These lines of evidence indicate that wedge 50S formed during MIS3 (Hamilton, Craig, and Sellmann 1988), not MIS2 (Lachniet, Lawson, and Sloat 2012). Given the recent use of DOC and CO_2 in radiocarbon dating ice wedges (Grinter et al. 2019; Kim et al. 2019; Vasil'chuk and Vasil'chuk 2017), it is important to resolve why radiocarbon dates on these materials from wedge 50S do not appear to be accurate. At present, we do not have a satisfactory explanation. The $\delta^{13}C$ values of CO_2 from within wedge 50S suggest much of the CO_2 is derived from decomposing organic material within the palaeo active layer that may be older than the ice wedge (Lachniet, Lawson, and Sloat 2012). Therefore, radiocarbon dates must be corrected based on estimations of atmospheric and respired CO_2 contributions, informed by $\delta^{13}C$ values. These corrections would result in a younger age estimate, though not likely as much as the offset between these studies. Similarly, radiocarbon dates from dissolved organic carbon and particulate carbon are more likely to be affected by 'old' carbon in permafrost settings. Therefore, the youngest radiocarbon dates are usually considered accurate estimates of the ice wedge's true age if contamination with modern carbon can be excluded, logic followed by Lachniet, Lawson, and Sloat (2012). The contradiction between this study and Lachniet, Lawson, and Sloat (2012) highlights the difficulties in directly dating ice wedges, which remains challenging (Vasil'chuk and Vasil'chuk 2017).

While we are confident that ice wedge 50S formed during MIS3, ice wedges elsewhere in the CRREL Tunnel may be younger. For example, in the South Tunnel silt is consistently dated to 35,000–31,000 cal yr BP and therefore intruding ice wedges must be younger and, in some case, may even have formed during the Holocene (Kanevskiy et al. 2022). The variable isotopic values of ice wedges suggest that several generations of ground ice are preserved throughout the tunnel and that they formed under different climates (Douglas et al. 2011, 2025; Kanevskiy et al. 2022).

Synthesized stratigraphy and chronology

Our eight exposures can be placed within three previously described late Pleistocene cryostratigraphic units that are found throughout the CRREL Permafrost Tunnel (Hamilton, Craig, and Sellmann 1988; Kanevskiy et al. 2022). The composite sediment sequence spans approximately 45,000 to 31,000 cal yr BP (units one and two) and 16,000 cal yr BP to at least 13,400 cal yr BP (unit three), with a substantial hiatus during MIS2. Here, we describe these cryostratigraphic

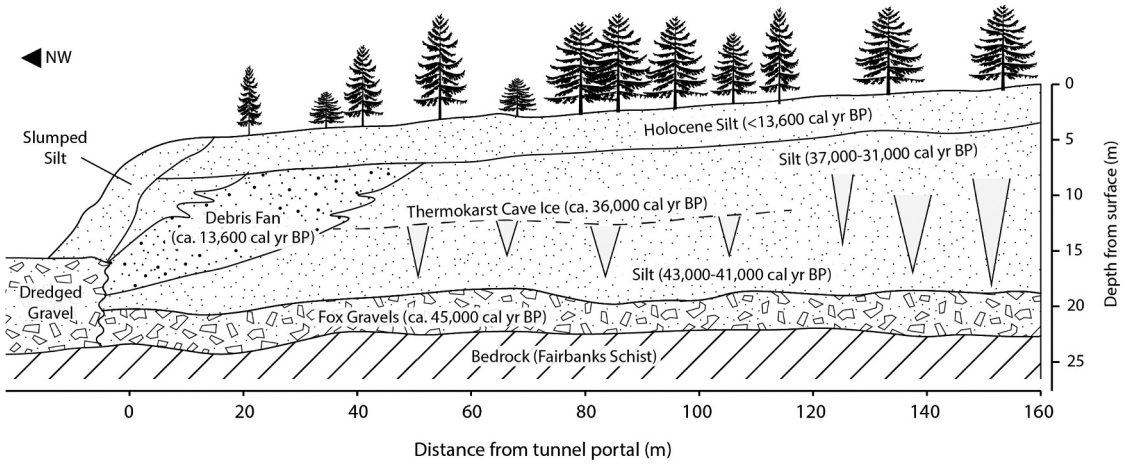

Figure 11. Simplified stratigraphy of the CRREL Tunnel Complex. Re-drawn from Hamilton, Craig, and Sellmann (1988), Kanevskiy et al. (2022), and Douglas et al. (2025). Date estimates are taken from this study. Note that neither the older silt (43,000–38,000 cal yr BP) nor Debris Fan are exposed in the South Tunnel.

units with reference to previous interpretations and new findings from this study (Figure 11).

Unit one (Fox Gravel)

Unit one is formed of the Fox Gravel previously described by Péwé (1975) and Hamilton, Craig, and Sellmann (1988). The unit is present throughout exposure six and at the base of exposure four where it is overlain by fluvial deposits interbedded with the fine-grained (loessal) sediments. Previous radiocarbon dating efforts at the CRREL Tunnel and new data from this study show the Fox Gravels were deposited during MIS3, ca. 45,000 cal yr BP (Sellmann 1972; Hamilton, Craig, and Sellmann 1988; Long and Péwé 1996; Tables 1, S2, S3).

Unit two (Pleistocene silt)

Unit two is composed of late Pleistocene silt described by Sellmann (1967, 1972), Hamilton, Craig, and Sellmann (1988) and Kanevskiy et al. (2022). The unit is present at exposures throughout the tunnel complex, including exposures one, two, three, four, five, and seven. The base of the silt is visible at exposure four where the transition from fluvial to eolian deposition is radiocarbon dated to ca. 43,000 cal yr BP. Large ice wedges up to 2 m wide are present throughout unit two, and in the North Tunnel are truncated at a common depth that can be traced along the tunnel walls. The truncated ice wedges represent a period of thaw and a slowing of silt accumulation ca. 36,000 cal yr BP, often associated with thermokarst cave ice. In several sections there appears to be a hiatus of several thousand years before silt accumulation resumes and continues until ca. 31,000 cal yr BP. Hamilton, Craig, and Sellmann (1988) suggest that this hiatus marks a separation between two distinct units. In contrast, Shur et al. (2004) and Kanevskiy et al. (2022) argue that Pleistocene silt deposits throughout the tunnel complex can be combined into one continuous unit. Although there are differences in palaeoenvironmental data (e.g., CN, $\delta^{15}N$, and pore ice $\delta^{18}O$ values; Figure 12) before and after the period of thaw, ca. 36,000 cal yr BP, there is very little variance in the physical properties of the silt (e.g., particle size, ice content, and organic content; Hamilton, Craig, and Sellmann 1988; Kanevskiy et al. 2022; Tables S1, Fig. S6). In the South Tunnel and adjacent boreholes, no evidence of separate silt units has been observed. Some ice wedges are truncated, which indicates unevenly distributed unconformities, but there are also numerous ice wedges extending from the ceiling to the floor, and vertical extent of some wedges encountered by boreholes is ~10 m, which suggests their syngenetic nature (Kanevskiy et al. 2022). We therefore consider the late Pleistocene silt to represent one unit.

Unit three (Debris Fan deposits)

Unit three represents the Debris Fan deposits described by Hamilton, Craig, and Sellmann (1988). The unit is only present near the entrance of the North Tunnel and dissects exposure seven and caps exposure one. New AMS radiocarbon dates on *Salix* shrub macrofossils from the Debris Fan date to ca. 13,700 cal yr BP (Tables 1, S2), consistent with previous estimates (Sellmann 1967). Megafauna fossils from within debris fan are AMS radiocarbon dated to ca. 16,000 cal yr BP, and are older than woody plant macrofossil remains from the same unit. Sellmann (1967) reported similar results; however, these were later described as potentially unreliable by Hamilton, Craig, and Sellmann

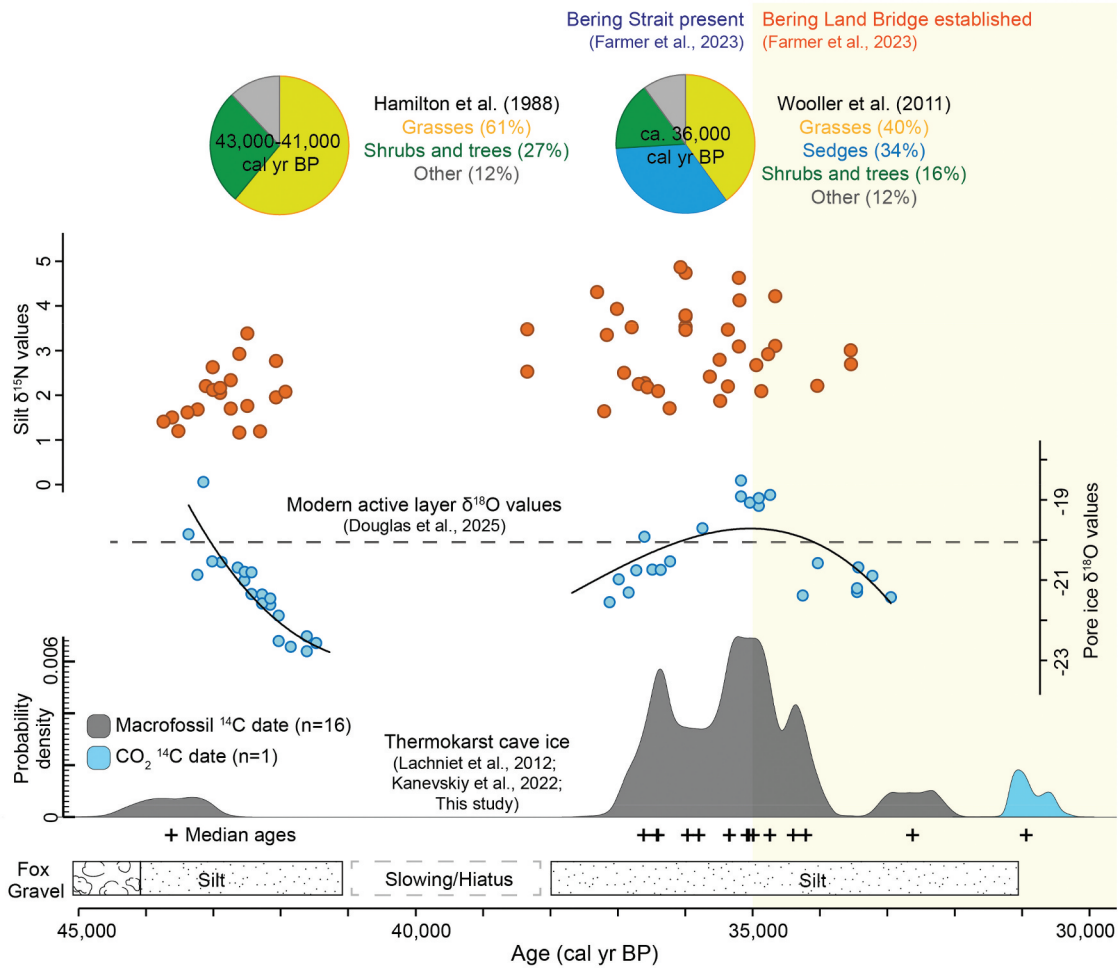

Figure 12. Palaeoenvironmental data from the CRREL Tunnel including pollen data, pore ice $\delta^{18}O$ values, silt $\delta^{15}N$ values, and sum probability of AMS radiocarbon dates on terrestrial macrofossils and CO_2 retrieved from thermokarst cave ice (Lachniet, Lawson, and Sloat 2012; Kanevskiy et al. 2022; this study).

(1988) because of inconsistencies in the bulk carbon technique used in 1966. Our replication of Sellmann's (1967) radiocarbon dating suggests that megafauna remains in the debris fan are derived from older, reworked deposits. This finding is consistent with the interpretations of Hopkins (1982) and Hamilton, Craig, and Sellmann (1988) who describe a widespread network of gullies in the Fairbanks areas that became active at the end of Pleistocene as permafrost thawed. At the CRREL Tunnel, clasts of schist in the Debris Fan show that upslope gullies must have eroded through thick loess to reach the underlying bedrock as material was transported toward the Goldstream Creek valley floor (Hamilton, Craig, and Sellmann 1988).

Palaeoenvironmental data

Radiocarbon-dating from this study and previous work allows us to place new and existing palaeoenviromental data (e.g., pollen, insects and plant macrofossils; Hamilton, Craig, and Sellmann 1988; Wooller et al. 2011) from the CRREL Tunnel into a robust chronology (Figure 12). Data span two portions of MIS3; 45,000–41,000 and 36,000–31,000 cal yr BP, as well as the latest Pleistocene, ca. 13,600 cal yr BP, and Early-Mid Holocene.

Macrofossil evidence from the Fox Gravel shows tall *Salix* shrubs grew on the floodplain of Goldstream Creek, ~45,000 cal yr BP (Figure 8). Pollen data suggests that *Betula* was also present, along with graminoids, monolete ferns and a range of herbaceous taxa (Hamilton, Craig, and Sellmann 1988). Limited comparative ecological data from interior Alaska is available for this period, which remains poorly understood because of the difficulties in dating deposits of this age (Monteath et al. 2025). Gaglioti et al. (2011) report macrofossil evidence from an arctic ground squirrel midden retrieved from Engineer Creek, near Fairbanks, and

radiocarbon-dated to ~44,000 cal yr BP. The remains of Poaceae (48 percent) and *Carex* spp. (32 percent) dominate the assemblage, however, the radiocarbon date is unreplicated and should be treated with caution as it lies near the practical limit of the technique. Elsewhere in eastern Beringia, a limited number of Yedoma deposits and lake-sediment records that can be approximately dated to ~45,000 cal yr BP suggest environments were characterized by gallery forests and shrub tundra (Anderson et al. 1994; Berger and Anderson 2000; Mahony 2015). High *Betula* values (10–40 percent) are present in pollen records; however, *Alnus* is virtually absent, suggesting moisture levels were lower than present.

Paleaoecological evidence from lower in the Pleistocene silt indicates that between 43,000–41,000 cal yr BP the local environment was an open meadow occupied by grasses, sedges and shrubs. Poaceae (61 percent), *Betula* (18 percent), and *Alnus* (9 percent) form the majority of pollen data from lower silt and plant macrofossils are represented by an abundance of *Carex* and *Salix*. The insect assemblage generally agrees with a relatively dry and open meadow environment by dominance of the dry tundra weevil *Lepidophorus lineaticollis*, and the presence of the carabid *Trichocellus mannerheimi*. However, cold and wet conditions are indicated by the presence of the oribatid mite *Svalbardia lucens* (synonym *Oromurica lucens*) which has been recorded from wet meadows with *Carex* in northern Canada and grass-sedge tundra in northern coastal Alaska (Hamilton, Craig, and Sellmann 1988; Ermilov, Makarova, and Behan-Pelletier 2022, and references therein). Pore ice $\delta^{18}O$ values decline through this period from approximately −20.0 to −22.5‰. The $\delta^{18}O$ values from ice wedges (including ice wedge 50S; Lachniet, Lawson, and Sloat 2012) in silt dated to 43,000–41,000 cal yr BP are lower than those from Holocene ice wedges at the CRREL Tunnel (average −23.97; Kanevskiy et al. 2022), suggesting winter temperatures were colder during this period. Again, comparative data from interior Alaska is scarce, however, radiocarbon-dated fossils from grazing megafauna (woolly mammoth, steppe-bison and horse) are present in some abundance in the deposits around Fairbanks, suggesting wider herbaceous/graminoid environments (Guthrie 2001, 2006). Pore ice $\delta^{18}O$ values from Yedoma exposures in Yukon indicate that temperatures were cooler than today, but not as cold as the following Last Glacial Maximum (Mahony 2015). In northern Alaska, lake-sediment records suggest a continuation of shrub tundra (Anderson et al. 1994; Berger and Anderson 2000).

Radiocarbon-dated macrofossils from thermokarst cave ice cluster around 36,000–35,000 cal yr BP. At the same time pore ice $\delta^{18}O$ values in the CRREL Tunnel reach their MIS3 maximum (around −19‰); close to $\delta^{18}O$ values from the modern active layer (Figure 12). Thermokarst cave ice in the CRREL Tunnel is associated with surficial and underground erosion (Lewkowicz et al. 2025), which resulted in truncated ice-wedges and slumping features. The occurrence of these features has been used as evidence for the Fox Thermal Event, a brief regional warming period close to the end of MIS3 that is evident in other records from interior Alaska (e.g., Berger 2003), and may also be recorded in western Beringia (Anderson and Lozhkin 2001; Wetterich et al. 2014). Alternatively, Shur et al. (2004) and Bray, French, and Shur (2006) suggest cave ice formed during local gully erosion caused by spring snow melt, which does not require a climate-based explanation. The occurrence of thermokarst cave ice with maximum pore and segregated ice $\delta^{18}O$ values suggests cave ice formed during the warmest period of MIS3 evident at the CRREL Tunnel, implying at least a partial climatic role. *Salix* leaves trapped within the cave ice show that willow continued to be present locally (Figure 7).

In the North Tunnel, a well-preserved vegetation mat described by Wooller et al. (2011) lies immediately above thermokarst cave ice. Radiocarbon-dating by Wooller et al. (2011) and this study (Table 1) consistently date the vegetation mat to ca. 36,000 cal yr BP and it is likely contemporaneous with the underlying cave ice. Pollen from the mat is dominated by graminoids (Cyperaceae and Poaceae) and also includes abundant forb taxa (Figure 12). Pollen data suggest no trees were growing locally; however, small stands of spruce, alder, or birch may have been present in the region. Insect remains include taxa associated with both mesic and arid environments, with several important indicators of aquatic and riparian habitats like *Helophorus splendidus* and *Elaphrus parviceps*. Interestingly, sequential $\delta^{13}C$ analyses conducted along graminoid leaves indicate seasonal changes in water use efficiency, which Wooller et al. (2011) attribute to a reliance on winter precipitation. Together, these data suggest a diverse graminoid and herb-dominated habitat supported by seasonal snowmelt. It is likely that this unusual assemblage at least partially reflects micro-habitats amongst active ice-wedge polygons (Hamilton, Craig, and Sellmann 1988). Comparative pollen, macrofossil and insect data for this time period come from a continuous sequence at Isabella Basin,

near Fairbanks (Matthews Jr. 1974; dating replicated by Elias 2000). These data differ from those reported by Wooller et al. (2011) despite being of similar age (ca. 36,000 cal yr BP) and separated by only 6 km and 45 m elevation. Matthews Jr. (1974) report abundant *Picea* and *Betula* pollen and suggest conditions were similar to present-day taiga. It is plausible that the forest near the end of MIS3 was limited to the larger river-valley systems (Monteath et al. 2025), such as the Chena and Tanana drainage, which includes Isabella Basin; however, the chronology of Isabella Basin requires further scrutiny.

Lower pore ice $\delta^{18}O$ values and raised $\delta^{15}N$ values from higher in the Pleistocene silt suggests that between 36,000–33,000 cal yr BP temperatures and precipitation levels began to fall, although the temporal extent of the trend is limited. Pollen from woody taxa is also largely absent (Hamilton, Craig, and Sellmann 1988). These changes are consistent with the beginning of the MIS3-MIS2 transition. Summer insolation at 65 °N began to decline from ca. 35,000 cal yr BP. At the same time, the Bering Land Bridge became established and continued to expand as sea levels fell (Farmer et al. 2023). In eastern Beringia, these drivers pushed environments toward drier, less productive, conditions (Monteath et al. 2025). An absence of MIS2-aged silt is evident in borehole records drilled from above the CRREL Tunnel (Kanevskiy et al. 2022). This hiatus is observed elsewhere in interior Alaska as a slowing of loess accumulation and is linked with a combination of restricted regional MIS2 glaciation (relative to MIS4 and MIS6) and lower surface roughness of the steppe-tundra vegetation, which limited silt accumulation (Jensen et al. 2016; Muhs et al. 2003).

Younger palaeoenvironmental data come from the Debris Fan unit and are described by Hamilton, Craig, and Sellmann (1988) and include macrofossil evidence for moist substrates (e.g., gastropod shells and mosses) as well as abundant willow shrubs. Pore ice $\delta^{18}O$ values from silt immediately above the fan are amongst the highest observed at the CRREL Tunnel and are close to modern active layer values (Douglas et al. 2025). Four new radiocarbon dates from willow fossils are broadly consistent with previous dating (Hamilton, Craig, and Sellmann 1988; Sellmann 1967) and date the Debris Fan to ca. 13,600 cal yr BP. The fan formed during a period of rapid climate change as both temperatures and precipitation levels increased, leading to the collapse of the steppe-tundra, which was replaced first by shrub tundra and finally boreal forest (see Monteath et al. 2025 for review). In interior Alaska, these changes began ca. 14,000 cal yr BP and are captured by pollen data (Monteath et al. 2021), *sedaDNA* (Clarke et al. 2024), and lake level studies (Abbott et al. 2000; Barber and Finney 2000).

The sequence is capped by Early-Mid Holocene silt (Ready Bullion Formation; Péwé 1975a) that formed during periods of thermokarst which may have reworked older loess into valley bottoms (Hamilton, Craig, and Sellmann 1988). Gravimetric ice content is lower than the underlying Pleistocene silt and ice wedge $\delta^{18}O$ values (average –23.97‰) are higher than elsewhere in the CRREL Tunnel, reflecting higher Holocene temperatures (Kanevskiy et al. 2022).

Conclusions

The CRREL Tunnel is one of the best known Yedoma sequences in North America and preserves a rare Middle Wisconsinan (MIS3) palaeoenvironmental record. New chronology and sedimentology from eight exposures within the CRREL Tunnel shows the tunnel excavations dissect deposits that span 44,000–41,000 cal yr BP, 36,000–31,000 cal yr BP and the latest Pleistocene (ca. 13,400 cal yr BP). New dating of *in situ* macrofossils shows that radiocarbon dates on ice wedge CO_2 are likely to be inaccurate, highlighting the difficulty in dating these features. Our revised chronology places new and existing palaeoenviromental data into a framework that can be compared with wider records from eastern Beringia. Between 43,000–41,000 cal yr BP shrub tundra was present with occasional alder. Pore and segregated ice $\delta^{18}O$ values reach their maximum ca. 36,000 cal yr BP, coinciding with the formation of thermokarst cave ice and a slowing of silt accumulation. Later, between 35,000–31,000 cal yr BP herbs and sedges became more common and soil $\delta^{15}N$ values rose as and the Bering Land Bridge became established.

Acknowledgments

We would like to thank CRREL for site access and guidance around the tunnel complex. Evan Francis and Joel Pumple supported isotope and particle size analyses undertaken in the PACS laboratory. We are grateful to Tom Ager for the helpful discussions on the CRREL Tunnel pollen record. Wooller was supported by the National Science Foundation (NSF, OPP 2310505). Wooller was also supported by an Institutional Development Award (IDeA) from the National Institute of General Medical Sciences of the National Institutes of Health (NIH) under grant number P20GM103395. Kanevskiy was supported by the National Science Foundation (NSF, RISE

2126965). The content is solely the responsibility of the authors and does not necessarily reflect the official views of NSF of NIH. Thomas Opel and a second anonymous reviewer provided helpful reviews that improved the final manuscript.

Author contributions

A.J.M. wrote the manuscript. S.L.C., D.F., M.K., and A.J.M. undertook field work. S.L.C. and A.J.M. conducted $\delta^2H/\delta^{18}O$ measurements and radiocarbon preparation. A.J.M. developed Bayesian age-depth models. M.J.W. analysed $\delta^{13}C$ and $\delta^{15}N$. M.F.J.P. identified shrub macrofossils. D.F. conceived the research. All authors contributed to data interpretation and provided comments on the manuscript.

Disclosure statement

No potential conflict of interest was reported by the author(s).

ORCID

Alistair J. Monteath http://orcid.org/0009-0000-0199-9926
Scott L. Cocker http://orcid.org/0000-0003-0974-4666
Thomas A. Douglas http://orcid.org/0000-0003-1314-1905
Michael F.J. Pisaric http://orcid.org/0000-0003-3806-8986
Duane Froese http://orcid.org/0000-0003-1032-5944

Data availability statement

All data produced in the study is made available in supplementary data (Tables S1-S2). OxCal v.4 code is available in the supplementary material.

References

Abbott, M.B., B.P. Finney, M.E. Edwards, and K.R. Kelts. 2000. Lake-level reconstruction and paleohydrology of Birch Lake, central Alaska, based on seismic reflection profiles and core transects. *Quaternary Research* 53, no. 2: 154–66. doi:10.1006/qres.1999.2112.

Alaska Climate Research Center. 2022. Fairbanks International Airport (PAFA) historical data. Accessed January 15, 2022. https://akclimate.org/data

Anderson, P. M., P. J. Bartlein, and L. B. Brubaker. 1994. Late quaternary history of tundra vegetation in northwestern Alaska. *Quaternary Research* 41, no. 3: 306–15.

Anderson, P.M., and A.V. Lozhkin. 2001. The Stage 3 interstadial complex (Karginskii/middle Wisconsinan interval) of Beringia: Variations in paleoenvironments and implications for paleoclimatic interpretations. *Quaternary Science Reviews* 20, no. 1–3: 93–125. doi:10.1016/S0277-3791(00)00129-3.

Barber, V.A., and B.P. Finney. 2000. Late Quaternary paleoclimatic reconstructions for interior Alaska based on paleolake-level data and hydrologic models. *Journal of Paleolimnology* 24, no. 1: 29–41. doi:10.1023/A:1008113715703.

Berger, A., and M.F. Loutre. 1991. Insolation values for the climate of the last 10 million years. *Quaternary Science Reviews* 10, no. 4: 297–317. doi:10.1016/0277-3791(91)90033-Q.

Berger, G.W. 2003. Luminescence chronology of late Pleistocene loess-paleosol and tephra sequences near Fairbanks, Alaska. *Quaternary Research* 60, no. 1: 70–83. doi:10.1016/S0033-5894(03)00060-7.

Berger, G. W., and P. M. Anderson. 2000. Extending the geochronometry of arctic lake cores beyond the radiocarbon limit by using thermoluminescence. *Journal of Geophysical Research Atmospheres* 105: 15439–55.

Bray, M.T., H.M. French, and Y. Shur. 2006. Further cryostratigraphic observations in the CRREL permafrost tunnel, Fox, Alaska. *Permafrost and Periglacial Processes* 17, no. 3: 233–43. doi:10.1002/ppp.558.

Bronk Ramsey, C. 2008. Deposition models for chronological records. *Quaternary Science Reviews* 27: 42–60.

Bronk Ramsey, C. 2009a. Bayesian analysis of radiocarbon dates. *Radiocarbon* 51, no. 1: 337–360. doi:10.1017/S0033822200033865.

Bronk Ramsey, C. 2009b. Dealing with outliers and offsets in radiocarbon dating. *Radiocarbon* 51, no. 3: 1023–1045. doi:10.1017/S0033822200034093.

Bronk Ramsey, C., and S. Lee. 2013. Recent and planned developments of the program OxCal. *Radiocarbon* 55: 720–730. doi:10.2458/azu_js_rc.55.16215.

Brown, T.A., D.E. Nelson, J.S. Vogel, and J.R. Southon. 1988. Improved collagen extraction by modified Longin method. *Radiocarbon* 30, no. 2: 171–7. doi:10.1017/S0033822200044118.

Clarke, C.L., P.D. Heintzman, Y. Lammers, A.J. Monteath, N. H. Bigelow, J.D. Reuther, B.A. Potter, P.D. Hughes, I. G. Alsos, and M.E. Edwards. 2024. Steppe-tundra composition and deglacial floristic turnover in interior Alaska revealed by sedimentary ancient DNA (sedaDNA). *Quaternary Science Reviews* 334: 108672. doi:10.1016/j.quascirev.2024.108672.

Cocker, S.L., E. Francis, C. Wanket, A.J. Monteath, S. Kuzmina, D. Tirlea, B.J.L. Jensen, P.D. Heintzman, B. Shapiro, and D.G. Froese. 2026. A local record of latest Pleistocene shrub expansion and steppe-tundra persistence in east Beringia. *Quaternary Science Reviews* 388: 110081. doi:10.1016/j.quascirev.2026.110081.

De Martinez, L.T.H.A., A.V. Reyes, G.D. Zazula, D.G. Froese, B.J. Jensen, and J.R. Southon. 2019. Permafrost-preserved wood and bone: Radiocarbon blanks from Yukon and Alaska. *Nuclear Instruments and Methods in Physics Research Section B: Beam Interactions with Materials and Atoms* 455: 154–7. doi:10.1016/j.nimb.2018.12.032.

Douglas, T.A., A.J. Barker, A.J. Monteath, and D.G. Froese. 2025. A local meteoric water line for interior Alaska constrains paleoclimate from 40000 year old relict permafrost. *Environmental Research Letters* 20, no. 2: 024029. doi:10.1088/1748-9326/ada16b.

Douglas, T.A., D. Fortier, Y.L. Shur, M.Z. Kanevskiy, L. Guo, Y. Cai, and M.T. Bray. 2011. Biogeochemical and geocryological characteristics of wedge and thermokarst-cave ice in the CRREL permafrost tunnel, Alaska. *Permafrost and Periglacial Processes* 22, no. 2: 120–8. doi:10.1002/ppp.709.

Douglas, T.A., C.A. Hiemstra, J.E. Anderson, R.A. Barbato, K. L. Bjella, E.J. Deeb, A.B. Gelvin, et al. 2021. Recent degradation of Interior Alaska permafrost mapped with ground surveys, geophysics, deep drilling, and repeat airborne

LiDAR. *The Cryosphere* 15, no. 8: 3555–75. doi:10.5194/tc-15-3555-2021.

Douglas, T.A., M.T. Jorgenson, M.Z. Kanevskiy, V. E. Romanovsky, Y. Shur, and K. Yoshikawa. 2008. *Permafrost dynamics at the Fairbanks permafrost experimental station near Fairbanks, Alaska*. Fairbanks: University of Alaska.

Elias, S.A. 2000. Late Pleistocene climates of Beringia, based on analysis of fossil beetles. *Quaternary Research* 53, no. 2: 229–35. doi:10.1006/qres.1999.2093.

Ermilov, S.G., O.L. Makarova, and V.M. Behan-Pelletier. 2022. Taxonomy and ecology of the Arctic oribatid mite *Svalbardia lucens* comb. nov. (Acari, Oribatida, Ceratozetidae): resolving a long-standing confusion. *Systematic and Applied Acarology* 27, no. 3: 497–510.

Farmer, J.R., T. Pico, O.M. Underwood, R. Cleveland Stout, J. Granger, T.M. Cronin, F. Fripiat, A. Martínez-García, G. H. Haug, and D.M. Sigman. 2023. The Bering Strait was flooded 10,000 years before the Last Glacial Maximum. *Proceedings of the National Academy of Sciences* 120, no. 1: e2206742119. doi:10.1073/pnas.2206742119.

Froese, D.G., J.A. Westgate, A.V. Reyes, R.J. Enkin, and S. J. Preece. 2008. Ancient permafrost and a future, warmer Arctic. *Science* 321, no. 5896: 1648–1648. doi:10.1126/science.1157525.

Froese, D.G., G.D. Zazula, J.A. Westgate, S.J. Preece, P. T. Sanborn, A.V. Reyes, and N.J. Pearce. 2009. The Klondike goldfields and Pleistocene environments of Beringia. *GSA Today* 19, no. 8: 4–10. doi:10.1130/GSATG54A.1.

Froese, D., J. Westgate, S. Preece, and J. Storer. 2002. Age and significance of the late Pleistocene Dawson tephra in eastern Beringia. *Quaternary Science Reviews* 21, no. 20–22: 2137–42. doi:10.1016/S0277-3791(02)00038-0.

Gaglioti, B.V., B.M. Barnes, G.D. Zazula, A.B. Beaudoin, and M.J. Wooller. 2011. Late Pleistocene paleoecology of Arctic ground squirrel (*Urocitellus parryii*) caches and nests from Interior Alaska's mammoth steppe ecosystem, USA. *Quaternary Research* 76, no. 3: 373–82. doi:10.1016/j.yqres.2011.08.004.

Gaglioti, B.V., D.H. Mann, P. Groves, M.L. Kunz, L. M. Farquharson, R.E. Reanier, B.M. Jones, and M. J. Wooller. 2018. Aeolian stratigraphy describes ice-age paleoenvironments in unglaciated Arctic Alaska. *Quaternary Science Reviews* 182: 175–90. doi:10.1016/j.quascirev.2018.01.002.

Gärtner, H., S. Lucchinetti, and F.H. Schweingruber. 2015. A new sledge microtome to combine wood anatomy and tree-ring ecology. *IAWA* 36, no. 4: 452–9. doi:10.1163/22941932-20150114.

Griffing, C.Y. 2011. Pleistocene climate in Alaska from stable isotopes in an ice wedge. Master's thesis, University of Nevada, Las Vegas.

Grinter, M., D. Lacelle, N. Baranova, S. Murseli, and I. D. Clark. 2019. Late Pleistocene and Holocene ice-wedge activity on the Blackstone Plateau, central Yukon, Canada. *Quaternary Research* 91, no. 1: 179–93. doi:10.1017/qua.2018.65.

Guthrie, R.D. 1990. *Frozen fauna of the mammoth-steppe: The story of Blue Babe*. Chicago, Illinois: University of Chicago Press.

Guthrie, R.D. 2001. Origin and causes of the mammoth steppe: A story of cloud cover, woolly mammal tooth pits, buckles, and inside-out Beringia. *Quaternary Science Reviews* 20, no. 1–3: 549–74. doi:10.1016/S0277-3791(00)00099-8.

Guthrie, R.D. 2006. New carbon dates link climatic change with human colonization and Pleistocene extinctions. *Nature* 441, no. 7090: 207–9. doi:10.1038/nature04604.

Hamilton, T.D., J.L. Craig, and P.V. Sellmann. 1988. The Fox Permafrost Tunnel: A Late Quaternary Geologic Record in central Alaska. *Geological Society of America Bulletin* 100: 948–69. doi:10.1130/0016-7606(1988)100<0948:TFPTAL>2.3.CO;2.

Handley, L.L., A.T. Austin, G.R. Stewart, D. Robinson, C. M. Scrimgeour, J.A. Raven, T.H. Heaton, and S. Schmidt. 1999. The *15*N natural abundance (δ15N) of ecosystem samples reflects measures of water availability. *Australian Journal of Plant Physiology* 26, no. 2: 185–99. doi:10.1071/PP98146.

Heiri, O., A.F. Lotter, and G. Lemcke. 2001. Loss on ignition as a method for estimating organic and carbonate content in sediments: Reproducibility and comparability of results. *Journal of Paleolimnology* 25, no. 1: 101–10. doi:10.1023/A:1008119611481.

Hopkins, D.M. 1982. *Aspects of the paleogeography of Beringia during the late Pleistocene*. Paleoecology of Beringia.

Iizuka, Y., C. Miyamoto, S. Matoba, G. Iwahana, K. Horiuchi, Y. Takahashi, N. Kanna, K. Suzuki, and H. Ohno. 2019. Ion concentrations in ice wedges: An innovative approach to reconstruct past climate variability. *Earth and Planetary Science Letters* 515: 58–66. doi:10.1016/j.epsl.2019.03.013.

Jensen, B.J., M.E. Evans, D.G. Froese, and V.A. Kravchinsky. 2016. 150,000 years of loess accumulation in central Alaska. *Quaternary Science Reviews* 135: 1–23. doi:10.1016/j.quascirev.2016.01.001.

Jorgenson, M.T., T.A. Douglas, A.K. Liljedahl, J.E. Roth, T. C. Cater, W.A. Davis, G.V. Frost, P.F. Miller, and C. H. Racine. 2020. The roles of climate extremes, ecological succession, and hydrology in repeated permafrost aggradation and degradation in fens on the Tanana Flats, Alaska. *Journal of Geophysical Research: Biogeosciences* 125, no. 12: e2020JG005824. doi:10.1029/2020JG005824.

Jorgenson, M.T., C.H. Racine, J.C. Walters, and T. E. Osterkamp. 2001. Permafrost degradation and ecological changes associated with a warmingclimate in central Alaska. *Climatic Change* 48, no. 4: 551–79. doi:10.1023/A:1005667424292.

Jorgenson, M.T., K. Yoshikawa, M. Kanevskiy, Y. Shur, V. Romanovsky, S. Marchenko, G. Grosse, J. Brown, and B. Jones. 2008. Permafrost characteristics of Alaska. In *Proceedings of the ninth international conference on permafrost*, Vol. 3, pp. 121–2. Fairbanks: University of Alaska.

Kanevskiy, M., Y. Shur, N.H. Bigelow, K.L. Bjella, T. A. Douglas, D. Fortier, B.M. Jones, and M.T. Jorgenson. 2022. Yedoma Cryostratigraphy of Recently Excavated Sections of the CRREL Permafrost Tunnel Near Fairbanks, Alaska. *Frontiers in Earth Science* 9: 1312. doi:10.3389/feart.2021.758800.

Katayama, T., M. Tanaka, J. Moriizumi, T. Nakamura, A. Brouchkov, T.A. Douglas, M. Fukuda, F. Tomita, and K. Asano. 2007. Phylogenetic analysis of bacteria preserved in a permafrost ice wedge for 25,000 years. *Applied and*

Environmental Microbiology 73, no. 7: 2360–3. doi:10.1128/AEM.01715-06.

Kennedy, K.E., D.G. Froese, G.D. Zazula, and B. Lauriol. 2010. Last Glacial Maximum age for the northwest Laurentide maximum from the Eagle River spillway and delta complex, northern Yukon. *Quaternary Science Reviews* 29, no. 9–10: 1288–300. doi:10.1016/j.quascirev.2010.02.015.

Kim, K., J.W. Yang, H. Yoon, E. Byun, A. Fedorov, Y. Ryu, and J. Ahn. 2019. Greenhouse gas formation in ice wedges at Cyuie, central Yakutia. *Permafrost and Periglacial Processes* 30, no. 1: 48–57. doi:10.1002/ppp.1994.

Konert, M., and J.E.F. Vandenberghe. 1997. Comparison of laser grain size analysis with pipette and sieve analysis: A solution for the underestimation of the clay fraction. *Sedimentology* 44, no. 3: 523–35. doi:10.1046/j.1365-3091.1997.d01-38.x.

Lachniet, M.S., D.E. Lawson, and A.R. Sloat. 2012. Revised 14C Dating of Ice Wedge Growth in interior Alaska (USA) to MIS 2 Reveals Cold Paleoclimate and Carbon Recycling in Ancient Permafrost Terrain. *Quaternary Research* 78: 217–25. doi:10.1016/j.yqres.2012.05.007.

Lachniet, M.S., D.E. Lawson, H. Stephen, A.R. Sloat, and W. P. Patterson. 2016. Isoscapes of δ18O and δ2H reveal climatic forcings on Alaska and Yukon precipitation. *Water Resources Research* 52, no. 8: 6575–86. doi:10.1002/2016WR019436.

Lewkowicz, A.G., H.B. O'Neill, S.A. Wolfe, P. Roy-Léveillée, V.E. Roujanski, E. Hoever, S. Gruber, et al. 2025. Glossary of Permafrost Science and Engineering.

Linell, K.A. 1973. Long-term effects of vegetative cover on permafrost stability in an area of discontinuous permafrost. In *Proceedings of Permafrost: North American contribution to the Second International Conference*, 688–93. Washington, DC: National Academy of Sciences, National Research Council.

Liston, G.E., and C.A. Hiemstra. 2011. The changing cryosphere: Pan-Arctic snow trends (1979–2009). *Journal of Climate* 24, no. 21: 5691–712. doi:10.1175/JCLI-D-11-00081.1.

Long, A., and T.L. Péwé. 1996. Radiocarbon dating by high-sensitivity liquid scintillation counting of wood from the Fox permafrost tunnel near Fairbanks, Alaska. *Permafrost and Periglacial Processes* 7, no. 3: 281–5. doi:10.1002/(SICI)1099-1530(199609)7:3<281::AID-PPP222>3.0.CO;2-Y.

Mahony, M. E. 2015. 50,000 years of paleoenvironmental change recorded in meteoric waters and coeval paleoecological and cryostratigraphic indicators from the Klondike goldfields. PhD thesis., University of Alberta.

Mann, D.H., P. Groves, M.L. Kunz, R.E. Reanier, and B. V. Gaglioti. 2013. Ice-age megafauna in Arctic Alaska: Extinction, invasion, survival. *Quaternary Science Reviews* 70: 91–108. doi:10.1016/j.quascirev.2013.03.015.

Mann, D.H., D.M. Peteet, R.E. Reanier, and M.L. Kunz. 2002. Responses of an Arctic landscape to Lateglacial and early Holocene climatic changes: The importance of moisture. *Quaternary Science Reviews* 21, no. 8–9: 997–1021. doi:10.1016/S0277-3791(01)00116-0.

Matthews, J.V., Jr. 1974. Wisconsin environment of interior Alaska: Pollen and macrofossil analysis of a 27 meter core from the Isabella Basin (Fairbanks, Alaska). *Canadian Journal of Earth Sciences* 11, no. 6: 828–41. doi:10.1139/e74-083.

Meyer, H., L. Schirrmeister, A. Andreev, D. Wagner, H. W. Hubberten, K. Yoshikawa, A. Bobrov, et al. 2010a. Lateglacial and Holocene isotopic and environmental history of northern coastal Alaska–Results from a buried ice-wedge system at Barrow. *Quaternary Science Reviews* 29, no. 27–28: 3720–35. doi:10.1016/j.quascirev.2010.08.005.

Meyer, H., L. Schirrmeister, K. Yoshikawa, T. Opel, S. Wetterich, H.W. Hubberten, and J. Brown. 2010b. Permafrost evidence for severe winter cooling during the Younger Dryas in northern Alaska. *Geophysical Research Letters* 37, no. 3. doi:10.1029/2009GL041013.

Meyer, H., K. Yoshikawa, L. Schirrmeister, and A. Andreev 2008. The Vault Creek Tunnel (Fairbanks Region, Alaska) A Late Quaternary Palaeoenvironmental Permafrost Record. In *Ninth International Conference on Permafrost (NICOP)*, June-July 29-3, 2008, 1191–6. Fairbanks, Alaska: Conference Proceedings.

Monteath, A.J., B.V. Gaglioti, M.E. Edwards, and D. Froese. 2021. Late Pleistocene shrub expansion preceded megafauna turnover and extinctions in eastern Beringia. *Proceedings of the National Academy of Sciences* 118, no. 52: e2107977118. doi:10.1073/pnas.2107977118.

Monteath, A.J., M.E. Edwards, D. Froese, L. Anderson, B. V. Gaglioti, S.L. Cocker, J. Brigham-Grette, M.J. Wooller, B. Finney, and M.B. Abbott. 2025. Late quaternary environmental change in eastern Beringia. *Quaternary Science Reviews* 368: 109527.

Monteath, A.J., S. Kuzmina, M. Mahony, F. Calmels, T. Porter, R. Mathewes, P. Sanborn, et al. 2023. Relict permafrost preserves megafauna, insects, pollen, soils and pore-ice isotopes of the mammoth steppe and its collapse in central Yukon. *Quaternary Science Reviews* 299: 107878. doi:10.1016/j.quascirev.2022.107878.

Muhs, D.R., T.A. Ager, E.A. Bettis III, J. McGeehin, J.M. Been, J.E. Begét, M.J. Pavich, T.W. Stafford Jr, and D.A.S. Stevens. 2003. Stratigraphy and palaeoclimatic significance of Late Quaternary loess–palaeosol sequences of the Last Interglacial–Glacial cycle in central Alaska. *Quaternary Science Reviews* 22, no. 18–19: 1947–86. doi:10.1016/S0277-3791(03)00167-7.

Murchie, T.J., A.J. Monteath, M.E. Mahony, G.S. Long, S. Cocker, T. Sadoway, E. Karpinski, et al. 2021. Collapse of the mammoth-steppe in central Yukon as revealed by ancient environmental DNA. *Nature Communications* 12, no. 1: 1–18. doi:10.1038/s41467-021-27439-6.

Murton, J.B., and H.M. French. 1994. Cryostructures in permafrost, Tuktoyaktuk coastlands, western Arctic Canada. *Canadian Journal of Earth Sciences* 31, no. 4: 737–47. doi:10.1139/e94-067.

Murton, J.B., T. Opel, P. Toms, A. Blinov, M. Fuchs, J. Wood, A. Gärtner, et al. 2022. A multimethod dating study of ancient permafrost, Batagay megaslump, east Siberia. *Quaternary Research* 105: 1–22. doi:10.1017/qua.2021.27.

Newberry, R.J., T.K. Clautice, K.H. Combellick, R.A. Douglas, T. Laird, G.M. Liss, S.A. Pinney, D.S. Reifenstuhl, and D.N. Solie. 1996. *Preliminary Geologic Map of the Fairbanks Mining District*. Alaska: Alaska Division of Geological & Geophysical Surveys Public Data File. doi:10.14509/1740.

Nield, C.B., Y. Yanes, J.D. Reuther, D.R. Muhs, J.S. Pigati, J. H. Miller, and P.S. Druckenmiller. 2024. Late glacial–Younger Dryas climate in interior Alaska as inferred from

the isotope values of land snail shells. *Quaternary Research* 117: 119–34. doi:10.1017/qua.2023.54.

Péwé, T.L. 1975. *Quaternary geology of Alaska. U.S. Geological Survey Professional Paper 835*. US Government Printing Office.

Porter, T.J., D.G. Froese, S.J. Feakins, I.N. Bindeman, M. E. Mahony, B.G. Pautler, G.J. Reichart, P.T. Sanborn, M. J. Simpson, and J.W. Weijers. 2016. Multiple water isotope proxy reconstruction of extremely low last glacial temperatures in Eastern Beringia (Western Arctic). *Quaternary Science Reviews* 137: 113–25. doi:10.1016/j.quascirev.2016.02.006.

Porter, T.J., and T. Opel. 2020. Recent advances in paleoclimatological studies of Arctic wedge-and pore-ice stable-water isotope records. *Permafrost and Periglacial Processes* 31, no. 3: 429–41. doi:10.1002/ppp.2052.

Potter, B.A., J.D. Reuther, V.T. Holliday, C.E. Holmes, D. S. Miller, and N. Schmuck. 2017. Early colonization of Beringia and Northern North America: Chronology, routes, and adaptive strategies. *Quaternary International* 444: 36–55. doi:10.1016/j.quaint.2017.02.034.

Preece, S.J., J.A. Westgate, B.V. Alloway, and M.W. Milner. 2000. Characterization, identity, distribution, and source of late Cenozoic tephra beds in the Klondike district of the Yukon, Canada. *Canadian Journal of Earth Sciences* 37, no. 7: 983–96. doi:10.1139/e00-011.

Rabanus-Wallace, M.T., M.J. Wooller, G.D. Zazula, E. Shute, A.H. Jahren, P. Kosintsev, J.A. Burns, J. Breen, B. Llamas, and A. Cooper. 2017. Megafaunal isotopes reveal role of increased moisture on rangeland during late Pleistocene extinctions. *Nature Ecology and Evolution* 1, no. 5: 0125. doi:10.1038/s41559-017-0125.

Reimer, P.J., W.E. Austin, E. Bard, A. Bayliss, P.G. Blackwell, C.B. Ramsey, M. Butzin, et al. 2020. The IntCal20 Northern Hemisphere radiocarbon age calibration curve (0–55 cal kBP). *Radiocarbon* 62, no. 4: 725–57. doi:10.1017/RDC.2020.41.

Reyes, A.V., D.G. Froese, and B.J. Jensen. 2010. Permafrost response to last interglacial warming: Field evidence from non-glaciated Yukon and Alaska. *Quaternary Science Reviews* 29, no. 23–24: 3256–74. doi:10.1016/j.quascirev.2010.07.013.

Schirrmeister, L., H. Meyer, A. Andreev, S. Wetterich, F. Kienast, A. Bobrov, M. Fuchs, M. Sierralta, and U. Herzschuh. 2016a. Late Quaternary paleoenvironmental records from the Chatanika River valley near Fairbanks (Alaska). *Quaternary Science Reviews* 147: 259–78. doi:10.1016/j.quascirev.2016.02.009.

Schirrmeister, L., H. Meyer, A. Andreev, S. Wetterich, F. Kienast, A. Bobrov, M. Fuchs, M. Sierralta, and U. Herzschuh. 2016b. *Microscopic wood anatomy. Reprint of Schweingruber, F.H. 1990. Mikroskopische Holzanatomie. 3. Aufl. Birmensdorf, Eidgenössische Forschungsanstalt für Wald, Schnee und Landschaft. 226 S.*

Schweingruber, F. H. 2016. *Microscopic wood anatomy. Reprint of: Schweingruber FH (1990) Mikroskopische Holzanatomie.* 3rd edn. Eidgenössische Forschungsanstalt für Wald, Schnee und Landschaft, Birmensdorf.

Sellmann, P.V. 1967. *Geology of the USA CRREL permafrost tunnel*. Fairbanks, Alaska: Hanover, New Hampshire, U.S. Army CRREL Technical Report 199, 22.

Sellmann, P.V. 1972. Geology and properties of materials exposed in the USA CRREL permafrost tunnel: Hanover, New Hampshire, U.S. *Army CRREL Special Report* 177, no. 16.

Shur, Y., H.M. French, M.T. Bray, and D.A. Anderson. 2004. Syngenetic permafrost growth: Cryostratigraphic observations from the CRREL tunnel near Fairbanks, Alaska. *Permafrost and Periglacial Processes* 15, no. 4: 339–47. doi:10.1002/ppp.486.

Sloat, A. 2014. *Modern to Late Pleistocene Stable Isotope Climatology of Alaska*. UNLV Theses, Dissertations, Professional Papers, and Capstones

Vasil'chuk, Y.K., and A.C. Vasil'chuk. 2017. Validity of radiocarbon ages of Siberian yedoma. *GeoResJ* 13: 83–95. doi:10.1016/j.grj.2017.02.004.

Wendler, G., and M. Shulski. 2009. A century of climate change for Fairbanks, Alaska. *Arctic* 62, no. 3: 295–300.

Westgate, J.A., S.J. Preece, D.G. Froese, R.C. Walter, A. S. Sandhu, and C.E. Schweger. 2001. Dating early and middle (Reid) Pleistocene glaciations in central Yukon by tephrochronology. *Quaternary Research* 56, no. 3: 335–48. doi:10.1006/qres.2001.2274.

Wetterich, S., V. Tumskoy, N. Rudaya, A.A. Andreev, T. Opel, H. Meyer, L. Schirrmeister, and M. Hüls. 2014. Ice Complex formation in Arctic East Siberia during the MIS3 Interstadial. *Quaternary Science Reviews* 84: 39–55. doi:10.1016/j.quascirev.2013.11.009.

Wooller, M.J., G.D. Zazula, M. Blinnikov, B.V. Gaglioti, N. H. Bigelow, P. Sanborn, S. Kuzmina, and C. La Farge. 2011. The detailed palaeoecology of a mid-Wisconsinan interstadial (ca. 32 000 14C a BP) vegetation surface from interior Alaska. *Journal of Quaternary Science* 26, no. 7: 746–56. doi:10.1002/jqs.1497.

Wooller, M.J., G.D. Zazula, M. Edwards, D.G. Froese, R. D. Boone, C. Parker, and B. Bennett. 2007. Stable carbon isotope compositions of Eastern Beringian grasses and sedges: Investigating their potential as paleoenvironmental indicators. *Arctic, Antarctic, and Alpine Research* 39, no. 2: 318–31. doi:10.1657/1523-0430(2007)39[318:SCICOE]2.0.CO;2.

Zazula, G.D., D.G. Froese, C.E. Schweger, R.W. Mathewes, A. B. Beaudoin, A.M. Telka, C.R. Harington, and J.A. Westgate. 2003. Ice-age steppe vegetation in east Beringia. *Nature* 423, no. 6940: 603–603. doi:10.1038/423603a.